

Supplementary Material

The Bending of C₃: Experimentally Probing the *l*-type Doubling and Resonance

Marie-Aline Martin-Drumel Qiang Zhang Kirstin D. Doney Olivier Pirali
Michel Vervloet Dennis Tokaryk Colin Western Harold Linnartz
Yang Chen and Dongfeng Zhao

Contents

1 List of electronic files provided as supplementary material	3
2 Supplementary Tables and Figures	4
3 Analysis of the infrared spectrum: Determination of bend rovibrational energies	34
4 PGOPHER file	37
4.1 Hamiltonian	37
4.1.1 General definition of the Hamiltonian	37
4.1.2 Λ -doubling	37
4.1.3 States	38
4.2 External linelist files	39
4.3 Eigenvalues	39

List of Tables

S1	PGOPHER parameters found to better reproduce the $\tilde{\Lambda}^1\Pi_u - \tilde{X}^1\Sigma_g^+$ rovibronic bands of C ₃ observed in the present work	4
S2	$\tilde{\Lambda}^1\Pi_u - \tilde{X}^1\Sigma_g^+$ rovibronic bands of C ₃	5
S3	$\tilde{X}^1\Sigma_g^+ - \tilde{X}^1\Sigma_g^+$ rovibrational bands of C ₃	8
S4	Spectroscopic constants of C ₃ in the $\tilde{X}^1\Sigma_g^+$ and $\tilde{\Lambda}^1\Pi_u$	9
S5	Spectroscopic constants in the $\tilde{\Lambda}(000)$ perturber states	12

List of Figures

S1	Full FT-IR spectrum recorded in a methane discharge and comparison with a simulation of CO	13
S2	Portion of the experimental IR spectrum and comparison with simulations at rotational temperatures of 300, 500, and 700 K	14
S3	Overview of the $\tilde{\Lambda}(000) - \tilde{X}(040)$ band system	15
S4	Overview of the $\tilde{\Lambda}(020) - \tilde{X}(040)$ band system	15
S5	Overview of the $\tilde{\Lambda}(010) - \tilde{X}(050)$ band system	16
S6	Overview of the $\tilde{\Lambda}(000) - \tilde{X}(000)$ band system	16
S7	Overview of the $\tilde{\Lambda}(020) - \tilde{X}(000)$ band system	17
S8	Overview of the $\tilde{\Lambda}(040) - \tilde{X}(000)$ band system	18
S9	Overview of the $\tilde{\Lambda}(002) - \tilde{X}(000)$ band	19
S10	Overview of the $\tilde{\Lambda}(100) - \tilde{X}(000)$ band	19
S11	Overview of the $\tilde{\Lambda}(120) - \tilde{X}(000)$ band	20
S12	Overview of the $\tilde{\Lambda}(010) - \tilde{X}(010)$ $\Sigma_g^- - \Pi_u$ band	20
S13	Overview of the $\tilde{\Lambda}(010) - \tilde{X}(010)$ $\Delta_g - \Pi_u$ and $\Sigma_g^+ - \Pi_u$ bands	21
S14	Overview of the $\tilde{\Lambda}(020) - \tilde{X}(020)$ $\Pi_u^{(-)} - \Sigma_g^+$ and $\Pi_u^{(-)} - \Delta_g$ bands	22
S15	Overview of the $\tilde{\Lambda}(100) - \tilde{X}(020)$ $\Pi_u - \Sigma_g^+$ and $\Pi_u - \Delta_g$ bands	22
S16	Overview of the $\tilde{\Lambda}(010) - \tilde{X}(030)$ $\Delta_g - \Pi_u$ and $\Delta_g - \Phi_u$ bands	23
S17	Overview of the $\tilde{\Lambda}(100) - \tilde{X}(040)$ $\Pi_u - \Sigma_g^+$ and $\Pi_u - \Delta_g$ bands	23
S18	Overview of the (001)–(000) infrared band	24
S19	Overview of the (011)–(010) infrared band	25
S20	Overview of the (021)–(020) infrared bands	26
S21	Overview of the (031)–(030) infrared bands	27
S22	Overview of the (041)–(040) infrared bands	28
S23	Overview of the (051)–(050) infrared bands	29
S24	Q-branch in the (041)–(040) $\Gamma_u - \Gamma_g$ infrared band	30
S25	Zoom of the (031)–(030) $\Pi_g - \Phi_u$ and $\Phi_g - \Pi_u$ bands	31
S26	Zoom of the (041)–(040) $\Delta_u - \Gamma_g$ band	32
S27	Zoom of portions of the infrared spectrum	33

1 List of electronic files provided as supplementary material

- **ESIfiles.zip**

Contains:

- **C3combinedFit.pgo**
the PGOPHER file
- **[...].obs**
the observations files (linelists)
- **C3combinedFit.log**
the PGOPHER fit log file containing the residuals and final set of parameters.
- **energies.log**
the list of energy levels with J up to 55.

2 Supplementary Tables and Figures

Table S1: PGOPHER parameters found to better reproduce the $\tilde{A}^1\Pi_u - \tilde{X}^1\Sigma_g^+$ rovibronic bands of C_3 observed in the present work: approximate rotational temperatures (T_{rot} , derived using PGOPHER simulations, in K), full-width-at-half-maximum (FWHM, in cm^{-1} ; a Gaussian shape was used), and relative transition moment^a (t). The figure displaying an overview of each band is indicated in the last column (Figures without an “S” are located in the main paper).

Vibronic assignment		T_{rot}	FWHM	t	Figure
$\tilde{A}(000)-\tilde{X}(000)$	$\Pi_u-\Sigma_g^+$	70	0.03	1	S6
	$u\Sigma_u-\Sigma_g^+$	70 ^b	0.03	0 ^c	S6
	$uP_u-\Sigma_g^+$	70 ^b	0.03	0	S6
$\tilde{A}(020)-\tilde{X}(000)$	$\Pi_u^{(-)}-\Sigma_g^+$	20	0.02	1	S7
	$\Pi_u^{(+)}-\Sigma_g^+$	30	0.03	1	S7
$\tilde{A}(040)-\tilde{X}(000)$	$\Pi_u^{(-)}-\Sigma_g^+$	20	0.02	1	S8
	$\Pi_u^{(+)}-\Sigma_g^+$	20	0.02	1	S8
$\tilde{A}(002)-\tilde{X}(000)$	$\Pi_u-\Sigma_g^+$	20	0.02	1	S9
$\tilde{A}(100)-\tilde{X}(000)$	$\Pi_u-\Sigma_g^+$	20	0.02	1	S10
$\tilde{A}(120)-\tilde{X}(000)$	$\Pi_u-\Sigma_g^+$	20	0.02	1	S11
$\tilde{A}(010)-\tilde{X}(010)$	$\Sigma_g^--\Pi_u$	30	0.03	1	S12
	$\Delta_g-\Pi_u$	30	0.03	1	S13
	$\Sigma_g^+-\Pi_u$	30	0.03	1	S13
$\tilde{A}(000)-\tilde{X}(020)$	$\Pi_u-\Sigma_g^+$	70	0.03	1	3
	$\Pi_u-\Delta_g$	70	0.03	1	3
	$u\Sigma_u-\Sigma_g^+$	70 ^b	0.03	0	3
	$u\Sigma_u-\Delta_g$	70 ^b	0.03	0 ^d	3
	$uP_u-\Sigma_g^+$	70 ^b	0.03	0	3
$\tilde{A}(020)-\tilde{X}(020)$	$\Pi_u^{(-)}-\Sigma_g^+$	50	0.03	0.5	S14
	$\Pi_u^{(-)}-\Delta_g$	50	0.03	1	S14
$\tilde{A}(100)-\tilde{X}(020)$	$\Pi_u-\Sigma_g^+$	70	0.04	1	S15
	$\Pi_u-\Delta_g$	70	0.04	0.5	S15
$\tilde{A}(010)-\tilde{X}(030)$	$\Sigma_g^--\Pi_u$	150	0.04	1	4
	$\Sigma_g^--\Phi_u$	150	0.04	0	4
	$\Delta_g-\Pi_u$	100	0.04	1	S16
	$\Delta_g-\Phi_u$	100	0.04	0.2	S16
$\tilde{A}(000)-\tilde{X}(040)$	$\Pi_u-\Sigma_g^+$	150	0.04	1	S3
	$\Pi_u-\Delta_g$	150	0.04	0.1	S3
	$\Pi_u-\Gamma_g$	150	0.04	0	S3
$\tilde{A}(020)-\tilde{X}(040)$	$\Pi_u^{(-)}-\Sigma_g^+$	70	0.03	1	S4
	$\Pi_u^{(-)}-\Delta_g$	70	0.03	1	S4
	$\Pi_u^{(-)}-\Gamma_g$	70	0.03	0	S4
$\tilde{A}(100)-\tilde{X}(040)$	$\Pi_u-\Sigma_g^+$	70	0.03	1	S17
	$\Pi_u-\Delta_g$	70	0.03	0.5	S17
$\tilde{A}(010)-\tilde{X}(050)$	$\Delta_g-\Pi_u$	150	0.04	1	S5
	$\Delta_g-\Phi_u$	150	0.04	0.5	S5

^a The transition moments were not adjusted to reproduce qualitatively all the observed bands but only bands overlapping in a given spectral window. Typically, these rovibronic bands arise from $\tilde{X}^1\Sigma_g^+$ states with the same number of quanta of excitation in ν_2 , but with different l values, and reach the same $\tilde{A}^1\Pi_u - \tilde{X}^1\Sigma_g^+$ state.

^b Assumed to be the same as the main rovibronic band.

^c Bands with $t = 0$ are observed by perturbations.

^d Transitions involving levels with f symmetry in the lower state (odd J values) appear about 5 times weaker on the experimental spectrum than predicted by the simulation.

Table S2: $\tilde{\Lambda}^1\Pi_u - \tilde{X}^1\Sigma_g^+$ rovibronic bands of C₃ observed in the literature (when rovibronic assignments were provided) and this work. Data ruled out are excluded from the combined fit. ν_0 is the band center (in cm⁻¹) and J''_{\max} the highest J value in the lower state. Unc. is the typical uncertainty on line frequencies (in cm⁻¹; higher values may be used for specific lines because of blending or perturbations). Offset is the offset applied the dataset wavenumbers in the present fit (in cm⁻¹).

Vibronic assignment		Datasets				Combined fit		
	ν_0^a	Ref.	J''_{\max}	Unc. ^b	Offset ^c	Comments		
$\tilde{\Lambda}(000)-\tilde{X}(000)$	$\Pi_u-\Sigma_g^+$ 24676	Gausset et al. [1965]	64	0.02	+0.06			
		McCall et al. [2003]	14	0.005	+0.04			
		Zhang et al. [2005]	16	0.005	+0.03			
		Tanabashi et al. [2005]	64	0.005	0			
		Haddad et al. [2014]	26	0.02	0			
		Schmidt et al. [2014]	28	0.01	0	Å in air converted to cm ⁻¹ in vacuum		
		This work	24	0.002	0			
		McCall et al. [2003]	8	0.005	+0.04	lines assigned by Zhang et al. [2005]		
		Zhang et al. [2005]	14	0.005	+0.03			
		Haddad et al. [2014]	16	0.02	0			
$u\Sigma_u-\Sigma_g^+$ 24679		Schmidt et al. [2014]	8	0.01	0	Å in air converted to cm ⁻¹ in vacuum		
		This work	14	0.002	0			
		McCall et al. [2003]	4	0.005	+0.04	lines assigned by Tanabashi et al. [2005]		
		Zhang et al. [2005]	4	0.005	+0.03			
		Haddad et al. [2014]	8	0.02	0			
		Schmidt et al. [2014]	4	0.01	0	Å in air converted to cm ⁻¹ in vacuum		
		This work	6	0.002	0			
		McCall et al. [2003]	—	—	mis-assignment [Tokaryk and Chomiak, 1997]			
		Balfour et al. [1994]	—	—	mis-assignment [Tokaryk and Chomiak, 1997]			
		Schmidt et al. [2014]	8	0.01	0	Å in air converted to cm ⁻¹ in vacuum		
$uP_u-\Sigma_g^+$ 24676		Tokaryk and Chomiak [1997]	30	0.003	0			
		This work	14	0.002	0			
		Gausset et al. [1965]	50	0.02	+0.04			
		Schmidt et al. [2014]	8	0.01	0	Å in air converted to cm ⁻¹ in vacuum		
		This work	18	0.002	0			
		Gausset et al. [1965]	50	0.03	+0.04			
		Schmidt et al. [2014]	8	0.01	0	Å in air converted to cm ⁻¹ in vacuum		
		This work	14	0.002	0			
		$\Pi_u^{(+)}-\Sigma_g^+$ 25529	Schmidt et al. [2014]	4	0.01	-0.099 Å in air converted to cm ⁻¹ in vacuum		
		This work	16	0.002	0	heavily perturbed		
$\tilde{\Lambda}(040)-\tilde{X}(000)$	$\Pi_u^{(-)}-\Sigma_g^+$ 25441	Izuha and Yamanouchi [1998]	16	0.08	0			
		$\Sigma_u^+-\Sigma_g^+$ 25694	Izuha and Yamanouchi [1998]	14	0.16	0		
		$\tilde{\Lambda}(031)-\tilde{X}(000)$	Izuha and Yamanouchi [1998]	22	0.08	0		
		$\tilde{\Lambda}(051)-\tilde{X}(000)$	Izuha and Yamanouchi [1998]	—	—	not compatible with this work		
		$\tilde{\Lambda}(002)-\tilde{X}(000)$	Balfour et al. [1994]	10	0.02	+0.082 Å in air converted to cm ⁻¹ in vacuum		
		$\Pi_u-\Sigma_g^+$ 26347	Schmidt et al. [2014]	14	0.002	+0.064		
		This work	—	—	—			
		$\tilde{\Lambda}(033)-\tilde{X}(000)$	Izuha and Yamanouchi [1998]	14	0.08	0		
		$\tilde{\Lambda}(053)-\tilde{X}(000)$	Izuha and Yamanouchi [1998]	14	0.08	0		
		$\tilde{\Lambda}(100)-\tilde{X}(000)$	$\Pi_u-\Sigma_g^+$ 25761	Gausset et al. [1965]	28	0.03	+0.04	
$\tilde{\Lambda}(120)-\tilde{X}(000)$		Schmidt et al. [2014]	12	0.01	+0.114 Å in air converted to cm ⁻¹ in vacuum			
		This work	18	0.002	+0.123			
		$\Pi_u-\Sigma_g^+$ 26128	This work	20	0.002	0		
		$\tilde{\Lambda}(111)-\tilde{X}(000)$	$\Sigma_u^+-\Sigma_g^+$ 26770	Izuha and Yamanouchi [1998]	18	0.04	0	
		$\tilde{\Lambda}(113)-\tilde{X}(000)$	$\Sigma_u^+-\Sigma_g^+$ 28956	Izuha and Yamanouchi [1998]	12	0.04	0	
		$\tilde{\Lambda}(133)-\tilde{X}(000)$	$\Sigma_u^+-\Sigma_g^+$ 29660	Izuha and Yamanouchi [1998]	12	0.04	0	

Continued on next page

Table S2 – continued from previous page

Vibronic assignment		Datasets			Combined fit		
	ν_0^a	Ref.	J''_{\max}	Unc. ^b	Offset ^c	Comments	
$\tilde{\Lambda}(200)-\tilde{X}(000)$	$\Pi_u-\Sigma_g^+$	Balfour et al. [1994]			—	not compatible with the $\tilde{\Lambda}(200)-\tilde{X}(200)$ band of Merer [1967]	
$\tilde{\Lambda}(010)-\tilde{X}(010)$	$\Sigma_g^--\Pi_u$ 24749	Gausset et al. [1965] This work	47 17	0.02 0.002	+0.04 0		
	$\Delta_g-\Pi_u$ 24872	Gausset et al. [1965] This work	51 18	0.02 0.002	+0.04 0		
	$\Sigma_g^+-\Pi_u$ 25093	Gausset et al. [1965] This work	39 17	0.02 0.002	+0.04 0		
$\tilde{\Lambda}(030)-\tilde{X}(010)$	$\Sigma_g^--\Pi_u$ 25168	Gausset et al. [1965]	59	0.02	+0.04		
	$\Delta_g^{(-)}-\Pi_u$ 25203	Gausset et al. [1965]	29	0.10	+0.04		
$\tilde{\Lambda}(050)-\tilde{X}(010)$	$\Sigma_g^--\Pi_u$ 25586	Gausset et al. [1965]	41	0.03	+0.04	4 corrected frequency (258.. → 255.. MHz)	
	$\Delta_g^{(-)}-\Pi_u$	Balfour et al. [1994]			—	not included in the fit	
$\tilde{\Lambda}(000)-\tilde{X}(020)$	$\Pi_u-\Sigma_g^+$ 24543	Gausset et al. [1965] This work	50 26	0.03 0.005	+0.04 0		
	$\Pi_u-\Delta_g$ 24544	Gausset et al. [1965] This work	48 30	0.03 0.005	+0.04 0	only e symmetry in \tilde{X} state	
	$u\Sigma_u-\Sigma_g^+$ 25546	This work	14	0.005	0	all symmetries in \tilde{X} state	
	$u\Sigma_u-\Delta_g$ 25458	This work	14	0.005	0		
	$uP_u-\Sigma_g^+$ 25542	This work	6	0.005	0	Q branch tentative	
$\tilde{\Lambda}(020)-\tilde{X}(020)$	$\Pi_u^{(-)}-\Sigma_g^+$ 25906	Gausset et al. [1965]			—	mis-assignment [Tokaryk and Chomiak, 1997]	
		Tokaryk and Chomiak [1997] This work	28 26	0.003 0.005	0 0		
	$\Pi_u^{(-)}-\Delta_g$ 25906	Gausset et al. [1965]			—	mis-assignment [Tokaryk and Chomiak, 1997]	
		Tokaryk and Chomiak [1997] This work	30 25	0.003 0.005	0 0		
	$\Phi_u-\Delta_g$ 25047	Tokaryk and Chomiak [1997]	29	0.003	0		
	$\Pi_u^{(+)}-\Sigma_g^+$ 25396	Gausset et al. [1965]	36	0.03	+0.04	Q only	
	$\Pi_u^{(+)}-\Delta_g$ 25398	Gausset et al. [1965]	36	0.03	+0.04	Q only	
$\tilde{\Lambda}(040)-\tilde{X}(020)$	$\Pi_u^{(-)}-\Sigma_g^+$ 25308	Gausset et al. [1965]	50	0.03	+0.04	Q only	
	$\Pi_u^{(-)}-\Delta_g$ 25310	Gausset et al. [1965]	50	0.03	+0.04	Q only	
	$\Phi_u-\Delta_g$	Balfour et al. [1994]			—	not included in the fit	
$\tilde{\Lambda}(100)-\tilde{X}(020)$	$\Pi_u-\Sigma_g^+$ 25629	This work	26	0.005	+0.117		
	$\Pi_u-\Delta_g$ 25629	This work	23	0.005	+0.117		
$\tilde{\Lambda}(010)-\tilde{X}(030)$	$\Sigma_g^--\Pi_u$ 24605	Gausset et al. [1965] This work	35 34	0.03 0.005	+0.04 0		
	$\Sigma_g^--\Phi_u$ 24607	This work	30	0.005	0		
	$\Delta_g-\Pi_u$ 24728	Gausset et al. [1965] This work	30 28	0.03 0.005	+0.04 0		
	$\Delta_g-\Phi_u$ 24729	This work	25	0.005	0		
	$\Sigma_g^+-\Pi_u$ 24949	Gausset et al. [1965]	26	0.03	+0.04		
$\tilde{\Lambda}(030)-\tilde{X}(030)$	$\Sigma_g^--\Pi_u$ 25024	Gausset et al. [1965]	19	0.1	+0.04		
	$\Delta_g^{(-)}-\Pi_u$ 25060	Gausset et al. [1965]	29	0.1	+0.04	Q only	
$\tilde{\Lambda}(050)-\tilde{X}(030)$	$\Sigma_g^--\Pi_u$ 25442	Gausset et al. [1965]	27	0.03	+0.04		
$\tilde{\Lambda}(000)-\tilde{X}(040)$	$\Pi_u-\Sigma_g^+$ 24389	Gausset et al. [1965] This work	38 28	0.03 0.005	0 0		
	$\Pi_u-\Delta_g$ 24389	This work	28	0.005	0		
	$\Pi_u-\Gamma_g$ 24391	This work	30	0.005	0		
$\tilde{\Lambda}(020)-\tilde{X}(040)$	$\Pi_u^{(-)}-\Sigma_g^+$ 24752	This work	20	0.005	0		
	$\Pi_u^{(-)}-\Delta_g$ 24752	This work	21	0.005	0		

Continued on next page

Table S2 – continued from previous page

Vibronic assignment	ν_0 ^a	Ref.	Datasets			Combined fit	
			J''_{\max}	Unc. ^b	Offset ^c	Comments	
	$\Pi_u^{(-)}-\Gamma_g$	24754	This work	21	0.005	0	
	$\Pi_u^{(+)}-\Sigma_g^+$	25242	Gausset et al. [1965]	32	0.03	+0.04	Q only
$\tilde{\Lambda}(040)-\tilde{X}(040)$	$\Pi_u^{(-)}-\Sigma_g^+$	25154	Gausset et al. [1965]	28	0.03	+0.04	Q only
$\tilde{\Lambda}(100)-\tilde{X}(040)$	$\Pi_u-\Sigma_g^+$	25475	This work	24	0.005	+0.114	
	$\Pi_u-\Delta_g$	25475	This work	24	0.005	+0.114	
$\tilde{\Lambda}(010)-\tilde{X}(050)$	$\Delta_g-\Pi_u$	24565	This work	26	0.005	0	
	$\Delta_g-\Phi_u$	24656	This work	22	0.005	0	
$\tilde{\Lambda}(000)-\tilde{X}(060)$	$\Pi_u-\Sigma_g^+$	24217	Merer [1967]	26	0.05	0	Q only
$\tilde{\Lambda}(000)-\tilde{X}(100)$	$\Pi_u-\Sigma_g^+$	23451	Merer [1967]	34	0.05	+0.04	Q only
			Zhang et al. [2005]	20	0.01	0	
	$u\Sigma-\Sigma_g^+$	23455	Zhang et al. [2005]	14	0.01	0	
	$uP-\Sigma_g^+$	23450	Zhang et al. [2005]	6	0.01	0	
$\tilde{\Lambda}(002)-\tilde{X}(100)$	$\Pi_u-\Sigma_g^+$	25122	Tokaryk and Chomiak [1997]	36	0.007	0	
$\tilde{\Lambda}(100)-\tilde{X}(100)$	$\Pi_u-\Sigma_g^+$	24537	Merer [1967]	34	0.05	0	
$\tilde{\Lambda}(110)-\tilde{X}(110)$	$\Sigma_g^+-\Pi_u$	24927	Tokaryk and Chomiak [1997]	27	0.007	0	
$\tilde{\Lambda}(100)-\tilde{X}(200)$	$\Pi_u-\Sigma_g^+$	23326	Merer [1967]	30	0.05	0	
$\tilde{\Lambda}(102)-\tilde{X}(200)$	$\Pi_u-\Sigma_g^+$	25008	Tokaryk and Chomiak [1997]	30	0.007	0	
$\tilde{\Lambda}(200)-\tilde{X}(200)$	$\Pi_u-\Sigma_g^+$	24408	Merer [1967]	32	0.05	0	
$\tilde{\Lambda}(001)-\tilde{X}(001)$	$\Pi_g-\Sigma_u^+$	23177	Izuha and Yamanouchi [1995]	27	0.008	0	
$\tilde{\Lambda}(021)-\tilde{X}(001)$	$\Pi_g^{(-)}-\Sigma_u^+$	23526	Izuha and Yamanouchi [1995]	23	0.008	0	
	$\Pi_g^{(+)}-\Sigma_u^+$	24020	Izuha and Yamanouchi [1995]	17	0.08	0	
$\tilde{\Lambda}(101)-\tilde{X}(001)$	$\Pi_g-\Sigma_u^+$	24250	Izuha and Yamanouchi [1998]	15	0.08	0	

^a Approximate band origin values. For more accurate values, the reader is referred to the levels energies reported in Table S4.

^b Unc. is either the value reported by the authors or a value determined in this work from the rms of the subset of data (see text).

^c For the data of Gausset et al. [1965], the offset determined by Tanabashi et al. [2005] was applied to all data except for the $\tilde{\Lambda}(000)-\tilde{X}(000)$ and $\tilde{\Lambda}(000)-\tilde{X}(040)$ bands (see text).

Table S3: $\tilde{X}^1\Sigma_g^+ - \tilde{X}^1\Sigma_g^+$ rovibrational bands of C_3 observed in the literature and this work. ν_0 is the band center (in cm^{-1}) and J''_{\max} the highest J value in the lower state. Unc. is the typical uncertainty on line frequencies (in cm^{-1} ; higher values may be used for specific lines because of blending or perturbations).

Vibronic assignment	Datasets				Combined fit
	ν_0 ^a	Ref.	J''_{\max}	Unc. ^b	
$\tilde{X}(010)-\tilde{X}(000)$ $\Pi_u-\Sigma_g^+$ 63	Schmuttenmaer et al. [1990]	6	2–3e-5		partly in Matsumura et al. [1988]
	Gendriesch et al. [2003]	16	0.5–1.3e-5		
	Breier et al. [2016]	16	3e-7–7e-4		
$\tilde{X}(001)-\tilde{X}(000)$ $\Sigma_u^+-\Sigma_g^+$ 2040	Matsumura et al. [1988]	52	0.001		partly in Matsumura et al. [1988]
	Kawaguchi et al. [1989]	40	0.001		
	This work	60	0.0005–0.003		
$\tilde{X}(021)-\tilde{X}(000)$ $\Sigma_u^+-\Sigma_g^+$ 2134	Kawaguchi et al. [1989]	26	0.001–0.003		
$\tilde{X}(101)-\tilde{X}(000)$ $\Sigma_u^+-\Sigma_g^+$ 3260	Krieg et al. [2013]	26	0.0005–0.002		
	Schröder et al. [2018]	18	0.001		
$\tilde{X}(011)-\tilde{X}(010)$ $\Pi_g-\Pi_u$ 2015	Kawaguchi et al. [1989]	41	0.001		
	This work	60	0.0005–0.005		
$\tilde{X}(111)-\tilde{X}(010)$ $\Pi_g-\Pi_u$ 3267	Krieg et al. [2013]	17	0.0005–0.002		
$\tilde{X}(021)-\tilde{X}(020)$ $\Sigma_u^+-\Sigma_g^+$ 2001	Kawaguchi et al. [1989]	32	0.001		
	This work	54	0.001–0.005		
	$\Delta_u-\Delta_g$ 1994	Kawaguchi et al. [1989]	32	0.001	heavily perturbed
$\Sigma_u^+-\Delta_g$ 2003	This work	55	0.001–0.005		
	$\Delta_u-\Sigma_g^+$ 1992	This work	20	0.005	tentative assignment, not in fit
	This work	18	0.005		tentative assignment, not in fit
$\tilde{X}(031)-\tilde{X}(030)$ $\Pi_g-\Pi_u$ 1985	This work	51	0.001–0.003		
	$\Phi_g-\Phi_u$ 1976	This work	55	0.001–0.002	
	$\Pi_g-\Phi_u$ 1988	This work	23	0.002–0.004	
	$\Phi_g-\Pi_u$ 1973	This work	31	0.003	
$\tilde{X}(041)-\tilde{X}(040)$ $\Sigma_u^+-\Sigma_g^+$ 1973	This work	48	0.001–0.003		
	$\Delta_u-\Delta_g$ 1970	This work	49	0.001–0.005	
	$\Gamma_u-\Gamma_g$ 1960	This work	49	0.001–0.004	
	$\Gamma_u-\Delta_g$ 1956	This work	30	0.002	
	$\Delta_u-\Gamma_g$ 1974	This work	28	0.002	
$\tilde{X}(051)-\tilde{X}(050)$ $\Pi_g-\Pi_u$ 1961	This work	48	0.001–0.008		
	$\Phi_g-\Phi_u$ 1956	This work	34	0.002–0.005	
	H_g-H_u 1945	This work	44	0.001–0.005	
$\tilde{X}(102)-\tilde{X}(001)$ $\Sigma_g^+-\Sigma_u^+$ 3228	Schröder et al. [2018]	17	0.001–0.003		
$\tilde{X}(201)-\tilde{X}(100)$ $\Sigma_u^+-\Sigma_g^+$ 3235	Schröder et al. [2018]	20	0.001–0.003		
$\tilde{X}(202)-\tilde{X}(101)$ $\Sigma_g^+-\Sigma_u^+$ 3201	Schröder et al. [2018]	19	0.001–0.003		
$\tilde{X}(203)-\tilde{X}(102)$ $\Sigma_u^+-\Sigma_g^+$ 3168	Schröder et al. [2018]	20	0.001–0.003		
$\tilde{X}(301)-\tilde{X}(200)$ $\Sigma_u^+-\Sigma_g^+$ 3211	Schröder et al. [2018]	22	0.001–0.003		
$\tilde{X}(302)-\tilde{X}(201)$ $\Sigma_g^+-\Sigma_u^+$ 3176	Schröder et al. [2018]	17	0.001		
$\tilde{X}(303)-\tilde{X}(202)$ $\Sigma_u^+-\Sigma_g^+$ 3141	Schröder et al. [2018]	22	0.001–0.003		
$\tilde{X}(401)-\tilde{X}(300)$ $\Sigma_u^+-\Sigma_g^+$ 3188	Schröder et al. [2018]	20	0.001		
$\tilde{X}(402)-\tilde{X}(301)$ $\Sigma_g^+-\Sigma_u^+$ 3152	Schröder et al. [2018]	21	0.001–0.003		
$\tilde{X}(403)-\tilde{X}(302)$ $\Sigma_u^+-\Sigma_g^+$ 3117	Schröder et al. [2018]	12	0.001–0.003		
$\tilde{X}(501)-\tilde{X}(400)$ $\Sigma_u^+-\Sigma_g^+$ 3164	Schröder et al. [2018]	22	0.001		
$\tilde{X}(502)-\tilde{X}(401)$ $\Sigma_g^+-\Sigma_u^+$ 3129	Schröder et al. [2018]	17	0.001–0.003		
$\tilde{X}(601)-\tilde{X}(500)$ $\Sigma_u^+-\Sigma_g^+$ 3141	Schröder et al. [2018]	20	0.001–0.003		
$\tilde{X}(701)-\tilde{X}(600)$ $\Sigma_u^+-\Sigma_g^+$ 3118	Schröder et al. [2018]	20	0.001–0.003		

^a Approximate band origin values. For more accurate values, the reader is referred to the levels energies reported in Table S4.

^b Unc. is either the value reported by the authors or a value determined in this work from the rms of the subset of data (see text). For this work data, the minimum and maximum values of the uncertainties are reported.

Table S4: Spectroscopic constants of C₃ in the $\tilde{X}^1\Sigma_g^+$ and $\tilde{A}^1\Pi_u$ determined in this work (in cm⁻¹). Numbers in parentheses are 1σ deviation of the fit, in units of the last digit of the parameter.

Vibronic Level	Origin ^a	B	D ×10 ⁶	H ×10 ¹⁰	L ×10 ¹⁴	M ×10 ¹⁷	P ×10 ²¹	-q/2 ×10 ³	-q _D /2 ×10 ⁷	-q _H /2 ×10 ¹¹	-q _L /2 ×10 ¹⁴	-q _M /2 ×10 ¹⁸
$\tilde{X}(000)$	Σ_g^+		0.430 587 17(17)	1.5337(25)	1.905(17)	-1.599(32)						
$\tilde{X}(010)$	Π_u	63.416 591 12(48)	0.442 415 78(25)	2.3525(28)	2.675(23)	-2.060(53)		-2.850 533(79)	5.048(19)	-12.14(35)	2.52(21)	-2.66(37)
$\tilde{X}(020)$	Σ_g^+	132.800 29(78)	0.451 584 0(62)	2.419(10)	1.571(31)							
	Δ_g	133.035 64(82)	0.453 099 5(67)	2.929(14)	3.185(88)	-2.52(17)						
	$\langle \Sigma_g^+ \Delta_g \rangle$							-3.8250(16)	5.074(28)	-5.143(89)		
$\tilde{X}(030)$	Π_u	207.4240(11)	0.460 472 9(66)	2.6930(94)	1.799(45)	-0.465(76)		-5.1990(35)	5.928(60)	-5.20(20)		
	Φ_u	208.3943(15)	0.462 887 4(98)	3.248(18)	2.79(11)	-1.45(23)						
	$\langle \Pi_u \Phi_u \rangle$							4.5111(22)	-5.249(43)	4.79(14)		
$\tilde{X}(040)$	Σ_g^+	286.5641(13)	0.467 958(12)	2.762(21)	1.585(80)							
	Δ_g	287.2198(11)	0.468 951 8(86)	2.884(13)	1.569(51)							
	Γ_g	289.1579(22)	0.472 027(11)	3.527(15)	2.484(52)							
	$\langle \Sigma_g^+ \Delta_g \rangle$							6.1731(30)	-6.804(77)	9.52(56)	-1.17(14)	
	$\langle \Delta_g \Gamma_g \rangle$							-5.0522(30)	5.130(65)	-3.88(25)		
$\tilde{X}(050)$	Π_u	370.4479(18)	0.475 305(15)	3.064(26)	3.28(10)			-7.3000(90)	4.75(25)			
	Φ_u	372.0318(17)	0.477 088(16)	2.648(28)								
	H_u	375.121(12)	0.480 649(30)	4.448(64)	4.47(22)							
	$\langle \Pi_u \Phi_u \rangle$							6.9550(84)	-8.07(24)			
	$\langle \Phi_u H_u \rangle$							-5.228(27)	1.56(25)			
$\tilde{X}(060)$	Σ_g^+	457.686(71)	0.495 24(46)	3.74(59)								
$\tilde{X}(001)$	Σ_u^+	2040.019 61(45)	0.435 715 4(46)	4.399(14)	10.91(18)	-23.6(10)	3.35(28)	-2.25(29)				
$\tilde{X}(011)$	Π_g	2078.500 05(34)	0.449 941 1(28)	4.9876(69)	8.391(63)	-10.96(24)	0.674(35)					
$\tilde{X}(021)$	Σ_u^+	2133.887 98(83)	0.456 057 2(72)	2.855(17)	-1.25(16)	11.11(72)	-1.39(11)					
	Δ_u	2127.382 25(85)	0.461 614 2(68)	5.219(14)	6.868(89)	-5.74(17)						
	$\langle \Sigma_u^+ \Delta_u \rangle$							-4.8336(26)	7.403(32)	-6.909(93)		
$\tilde{X}(031)$	Π_g	2192.7404(12)	0.465 365 4(66)	3.4033(72)	1.832(22)			-6.3044(34)	8.281(58)	-7.06(19)		
	Φ_g	2184.6423(15)	0.471 842 2(91)	5.262(17)	5.62(11)	-3.77(21)						
	$\langle \Pi_g \Phi_g \rangle$							5.3862(49)	-6.695(63)	5.26(18)		
$\tilde{X}(041)$	Σ_u^+	2260.4086(13)	0.471 912(12)	3.163(21)	1.423(77)							
	Δ_u	2257.3574(12)	0.474 413 4(88)	3.710(12)	2.026(45)							
	Γ_u	2249.1678(23)	0.481 155(11)	5.320(18)	4.868(97)	-2.25(18)						
	$\langle \Sigma_u^+ \Delta_u \rangle$							7.1792(36)	-7.837(68)	5.34(25)		
	$\langle \Delta_u \Gamma_u \rangle$							-5.8022(69)	5.927(89)	-3.60(27)		
$\tilde{X}(051)$	Π_g	2332.0313(21)	0.479 248(15)	3.533(30)	3.195(85)			-8.3389(85)	6.48(22)			

Continued on next page

Table S4 – continued from previous page

Vibronic Level	Origin ^a	B	D ×10 ⁶	H ×10 ¹⁰	L ×10 ¹⁴	M ×10 ¹⁷	PP ×10 ²¹	-q/2 ×10 ³	-q _D /2 ×10 ⁷	-q _H /2 ×10 ¹¹	-q _L /2 ×10 ¹⁴	-q _M /2 ×10 ¹⁸
Φ_g	2327.8379(19)	0.483 022(16)	3.310(32)									
H_g	2320.292(12)	0.489 795(29)	6.069(51)	6.15(24)								
$\langle \Pi_g \Phi_g \rangle$								7.969(13)	-8.83(17)			
$\langle \Delta_g \Gamma_g \rangle$								-5.371(54)	0.81(23)			
$\tilde{X}(100)$	Σ_g^+	1224.5258(18)	0.424 997(14)	0.671(27)								
$\tilde{X}(101)$	Σ_u^+	3260.127 38(25)	0.424 205 1(23)	1.0983(43)								
$\tilde{X}(102)$	Σ_g^+	5268.400 97(75)	0.427 047(11)	2.814(37)								
$\tilde{X}(110)$	Π_u	E_{110}	0.434 00(16)						-1.976(21)			
$\tilde{X}(111)$	Π_g	3330.508 60(31)	0.435 426 6(65)	1.970(23)					2.5905(38)	-3.52(17)		
$\tilde{X}(200)$	Σ_g^+	2435.737(23)	0.421 623(22)	0.458(42)								
$\tilde{X}(201)$	Σ_u^+	4459.6227(18)	0.419 492(15)	0.589(27)								
$\tilde{X}(202)$	Σ_g^+	6460.663 66(64)	0.418 210 6(87)	0.905(21)								
$\tilde{X}(203)$	Σ_u^+	8436.102 64(89)	0.419 522(11)	2.087(33)								
$\tilde{X}(300)$	Σ_g^+	E_{300}	0.419 074(29)	0.464(77)								
$\tilde{X}(301)$	Σ_u^+	5647.003(23)	0.416 401(20)	0.427(35)								
$\tilde{X}(302)$	Σ_g^+	7635.5297(19)	0.414 101(17)	0.517(38)								
$\tilde{X}(303)$	Σ_u^+	9601.787 39(82)	0.412 467 2(99)	0.770(21)								
$\tilde{X}(400)$	Σ_g^+	E_{400}	0.416 861(28)	0.345(49)								
$\tilde{X}(401)$	Σ_u^+	$E_{300} + 3187.81591(55)$	0.413 969(26)	0.437(61)								
$\tilde{X}(402)$	Σ_g^+	8799.144(23)	0.411 231(20)	0.408(32)								
$\tilde{X}(403)$	Σ_u^+	10 752.3052(20)	0.408 818(30)	0.62(14)								
$\tilde{X}(500)$	Σ_g^+	E_{500}	0.414 840(20)									
$\tilde{X}(501)$	Σ_u^+	$E_{400} + 3164.46678(53)$	0.411 807(27)	0.310(42)								
$\tilde{X}(502)$	Σ_g^+	6316.535 50(82)	0.408 962(26)	0.534(61)								
$\tilde{X}(600)$	Σ_g^+	E_{600}	0.412 942(38)									
$\tilde{X}(601)$	Σ_u^+	$E_{500} + 3141.09139(51)$	0.409 788(20)									
$\tilde{X}(701)$	Σ_u^+	$E_{600} + 3117.61126(48)$	0.407 929(34)									
$\tilde{A}(000)$ ^b	Π_u	24 676.1193(26)	0.412 105 3(72)	0.1214(55) -0.199(11)				0.5373(56)	-6.73(16)	42.3(13)	-11.50(43)	11.26(49)
$\tilde{A}(010)$	Σ_g^-	24 811.763 55(70)	0.416 015 5(49)	0.3067(45)								
	Δ_g	24 936.295 75(52)	0.415 310 2(36)	0.3253(25)								
	Σ_g^+	25 156.146 56(79)	0.408 384 6(67)	0.2130(91)								
$\tilde{A}(020)$	$\Pi_u^{(-)}$	25 038.985 39(65)	0.418 510 1(83)	0.205(26) -1.17(22)				1.9249(12)				
	Φ_u	25 179.8089(13)	0.418 568 6(98)	0.382(13)								
	$\Pi_u^{(+)}$	25 529.360 00(77)	0.414 117 2(59)	0.2699(44)				-2.3330(39)	1.275(36)			

Continued on next page

Table S4 – continued from previous page

Vibronic Level	Origin ^a	B	D ×10 ⁶	H ×10 ¹⁰	L ×10 ¹⁴	M ×10 ¹⁷	PP ×10 ²¹	-q/2 ×10 ³	-q _D /2 ×10 ⁷	-q _H /2 ×10 ¹¹	-q _L /2 ×10 ¹⁴	-q _M /2 ×10 ¹⁸
̃A(030)	Σ_g^-	25 230.7632(58)	0.421 816(12)	0.6673(46)								
	$\Delta_g^{(-)}$	25 267.880(56)	0.400 46(56)	-8.5(15)	-0.61(11)							
̃A(040)	$\Pi_u^{(-)}$	25 441.375 68(88)	0.422 613(11)	1.462(27)	-1.30(14)			3.0300(62)	-7.10(13)			
	$\Pi_u^{(+)}$	26 297.5400(13)	0.421 530(39)	-7.136(96)				1.005(31)				
̃A(050)	Σ_g^-	25 648.6774(92)	0.427 053(34)	1.787(23)								
̃A(001)	Π_g	25 217.2071(29)	0.410 892(10)					2.0239(70)				
̃A(002)	Π_u	26 346.617 91(95)	0.407 138(17)	0.467(41)	1.28(25)			0.2995(30)				
̃A(011)	Σ_u^+	25 694.403(40)	0.411 39(28)									
̃A(021)	$\Pi_g^{(-)}$	25 565.9034(29)	0.416 646(12)					0.8987(86)				
	$\Pi_g^{(+)}$	26 060.227(34)	0.414 74(24)					1.16(15)				
̃A(031)	Σ_u^+	26 437.640(85)	0.418 25(89)									
̃A(051)	Σ_u^+	27 165.067(44)	0.421 19(20)									
̃A(033)	Σ_u^+	28 594.627(42)	0.440 59(45)									
̃A(053)	Σ_u^+	29 293.248(43)	0.459 90(51)									
̃A(100)	Π_u	25 761.856 60(60)	0.409 671 6(72)	1.73(14)				0.2795(47)	-0.74(11)			
̃A(101)	Π_g	26 289.869(35)	0.412 16(30)					-0.114(19)				
̃A(102)	Π_u	27 443.669(23)	0.405 536(36)	2.59(59)				0.162(13)				
̃A(110)	Σ_g^+	$E_{110} + 24927.2012(35)$	0.405 19(17)									
̃A(111)	Σ_u^+	26 769.470(18)	0.409 10(11)									
̃A(113)	Σ_u^+	28 956.223(24)	0.428 69(33)									
̃A(120)	Π_u	26 127.646 02(96)	0.415 405(15)	3.47(44)				1.8342(34)				
̃A(133)	Σ_u^+	29 659.464(22)	0.433 40(26)									
̃A(200)	Π_u	26 843.976(35)	0.406 589(53)									

^a For the $\tilde{\Lambda}^1\Pi_u$ states, absolute values may be affected by data offsets, see the main text.

^b For the constants in the $\tilde{\Lambda}(000)$ perturbing states, see Table S5.

Table S5: Spectroscopic constants in the $\tilde{\Lambda}(000)$ and perturber states determined in this work (in cm^{-1}). Numbers in parentheses are 1σ deviation of the fit, in units of the last digit of the parameter. Parameters without numbers in parenthesis are fixed in the fit.

		This work	Haddad et al. [2014]
$\text{u}\Sigma_u$	Origin	24 678.6453(78)	24 678.526(24)
	B	0.450 43(50)	0.420 39(43)
	$D \times 10^4$	1.454(21)	0.01
	$H \times 10^7$	3.209(43)	
	λ	-0.1	-0.1
	γ	0.3802(41)	0.6093(70)
	LS	1.6539(41)	0.661(29)
	$LSN^2 \times 10^3$	-1.062(24)	
$\text{u}P_u(f)$	Origin	24 675.5258(64)	24 675.136(50)
	B	0.304 33(51)	0.3069(30)
	a	0.5283(51)	0.461(32)
$\text{u}P_u(e)$	Origin	24 675.9776(29)	24 675.783(29)
	B	0.356 525(73)	0.3513(7)
	a	0.4006(11)	0.405(13)

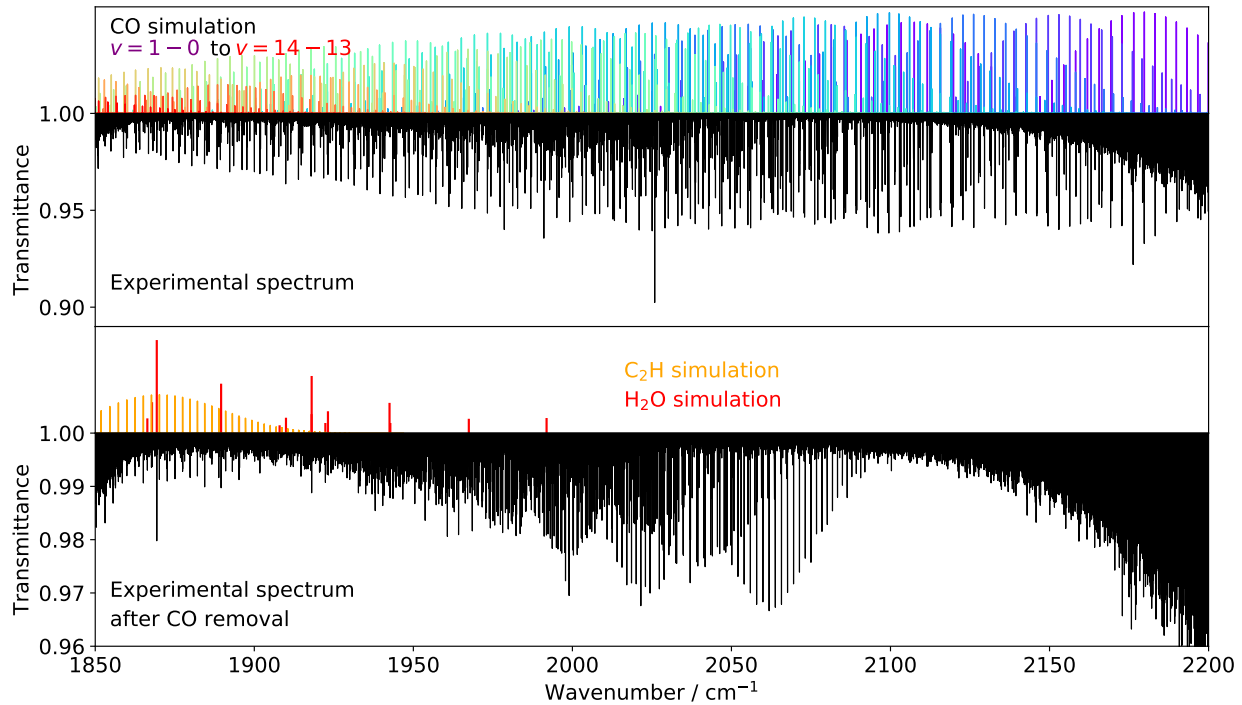


Figure S1: (*Top panel*) Full FT-IR spectrum recorded in a methane discharge and comparison with a simulation of CO $v = 1 - 0$ (in purple) to $v = 14 - 13$ (in red) bands at a rotational temperature of 500 K (simulations performed with the PGOPHER software). Under the assumption of thermal equilibrium, the relative intensity ratio between the fundamental and hot bands appears different than that of the experimental spectrum thus the intensity ratio between CO vibrational bands is set to qualitatively reproduce the experimental spectrum. The observed structure is in favor of a higher vibrational temperature, although no attempt has been made in this work to estimate it. (*Bottom panel*) FT-IR spectrum after removal of CO lines and comparison with simulation of the ν_2 band of H_2O (HITRAN at 300 K, in red), and the ν_3 band of C_2H (PGOPHER at 500 K, in orange). The intensity ratio between H_2O and C_2H vibrational bands is set to qualitatively reproduce the experimental spectrum. Most of the remaining transitions on the experimental spectrum arise from the C_3 species. The areas with lower transmittance toward each end of the frequency plot correspond to reduced transmission of our instrument (spectral filtering).

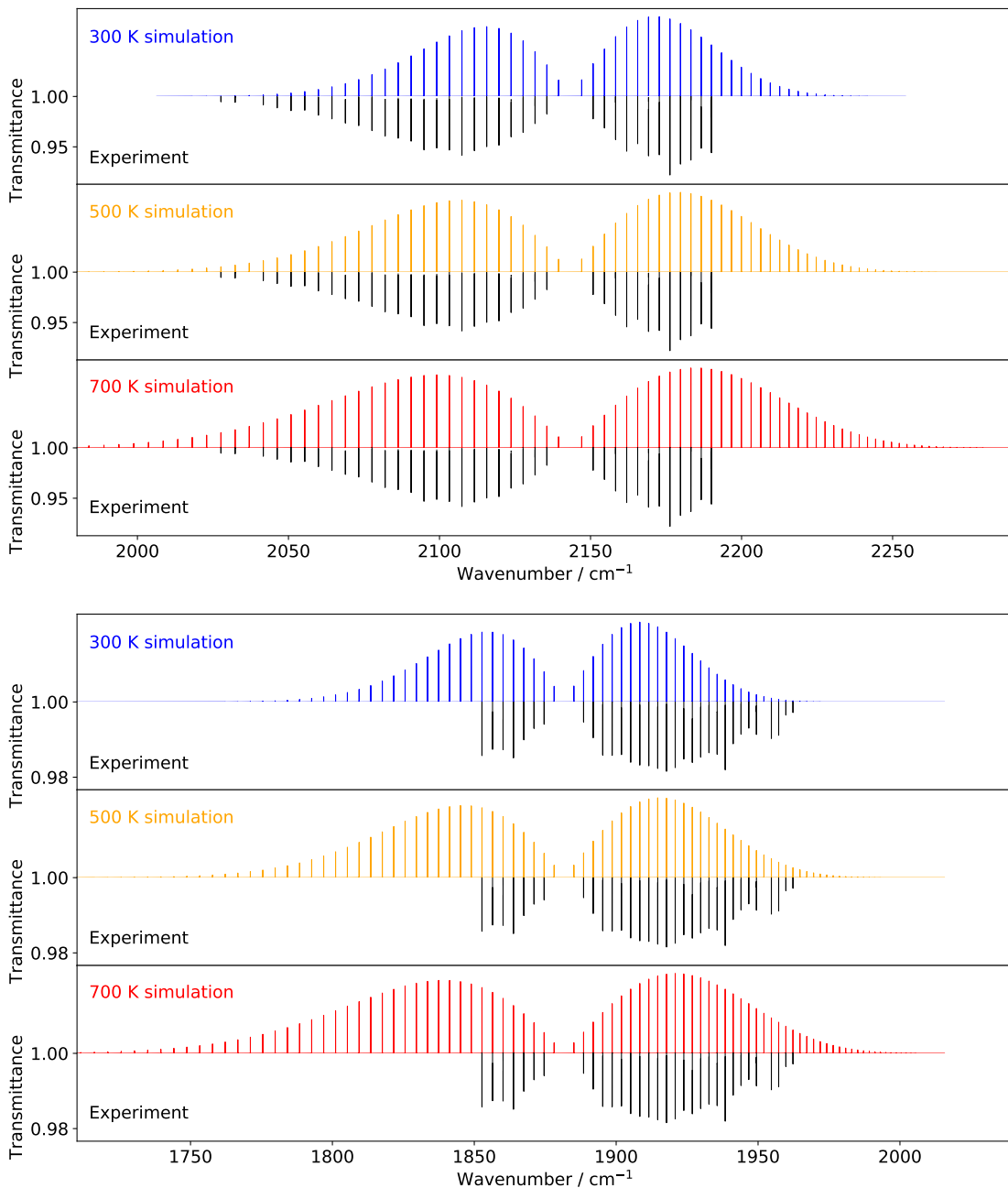
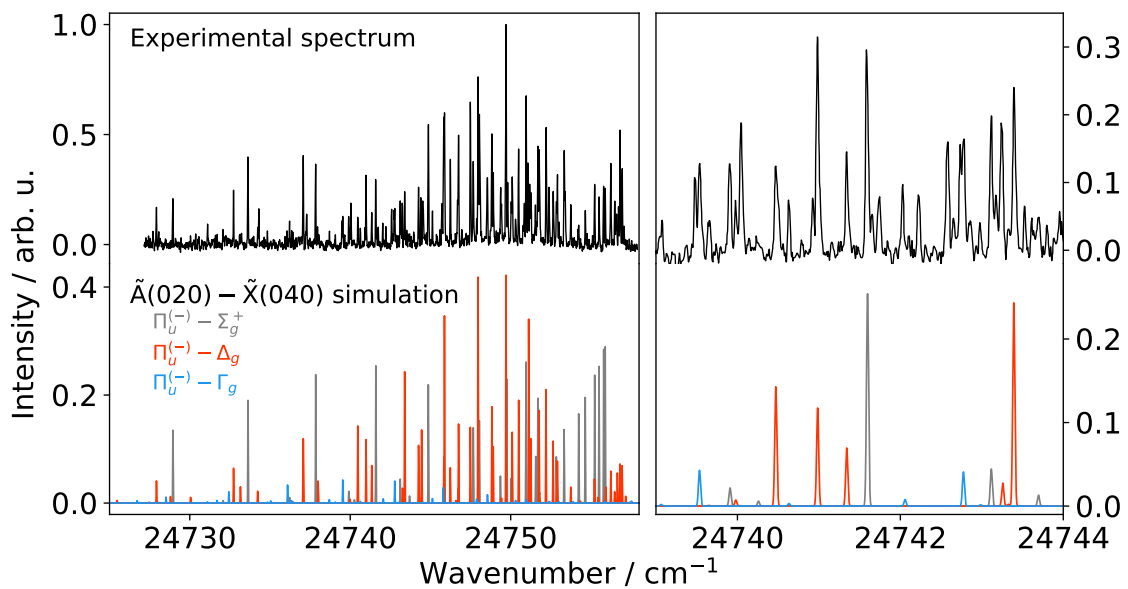
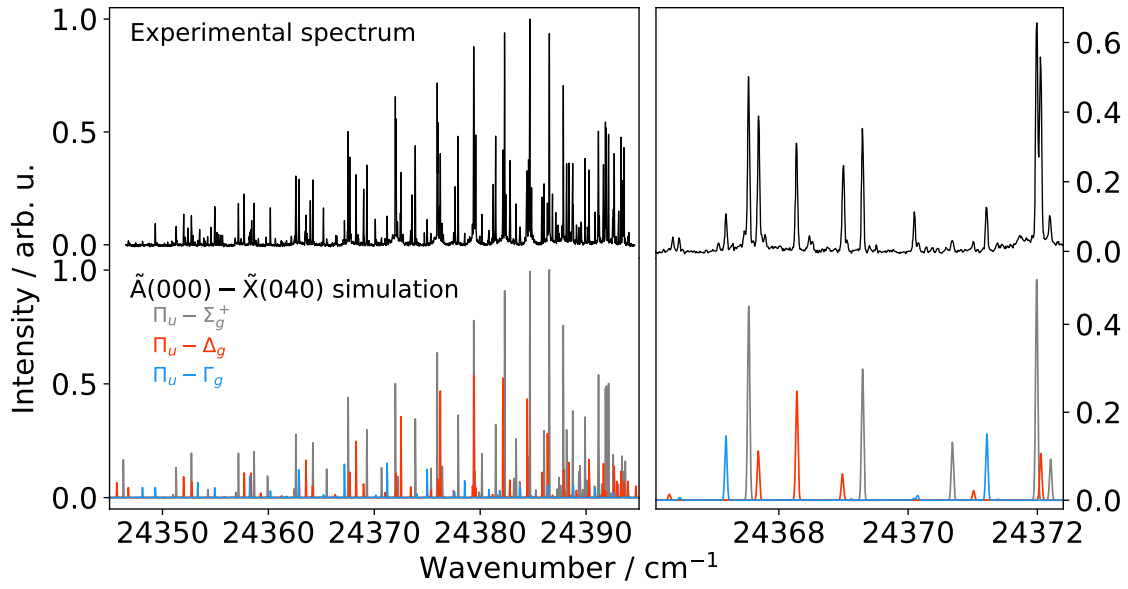


Figure S2: Portion of the experimental IR spectrum in which only the transitions assigned to the $v = 1 - 0$ (top panel) and $11 - 10$ (bottom panel) bands of CO are plotted, and comparison with simulations (in arbitrary units) at rotational temperatures of 300, 500, and 700 K. Simulations performed using the PGOPHER software. All intensities are in arbitrary units. A temperature of 500 K is found to better reproduce the rotational contour of the bands.



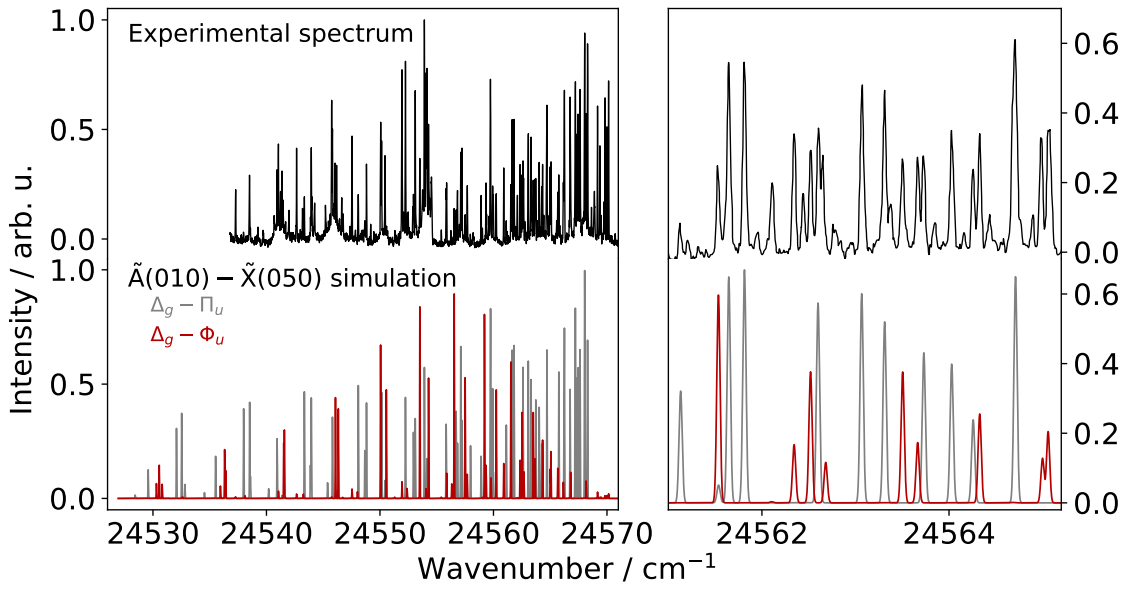


Figure S5: Overview of the $\tilde{A}(010) - \tilde{X}(050)$ band system (left panel), zoom of a portion of the spectral range (right panel) and comparison with a PGOPHER simulation at 150 K (lower traces). The R-branch intensity of the $\Delta_g - \Phi_u$ band appears significantly underestimated in the simulation compared to the experimental trace.

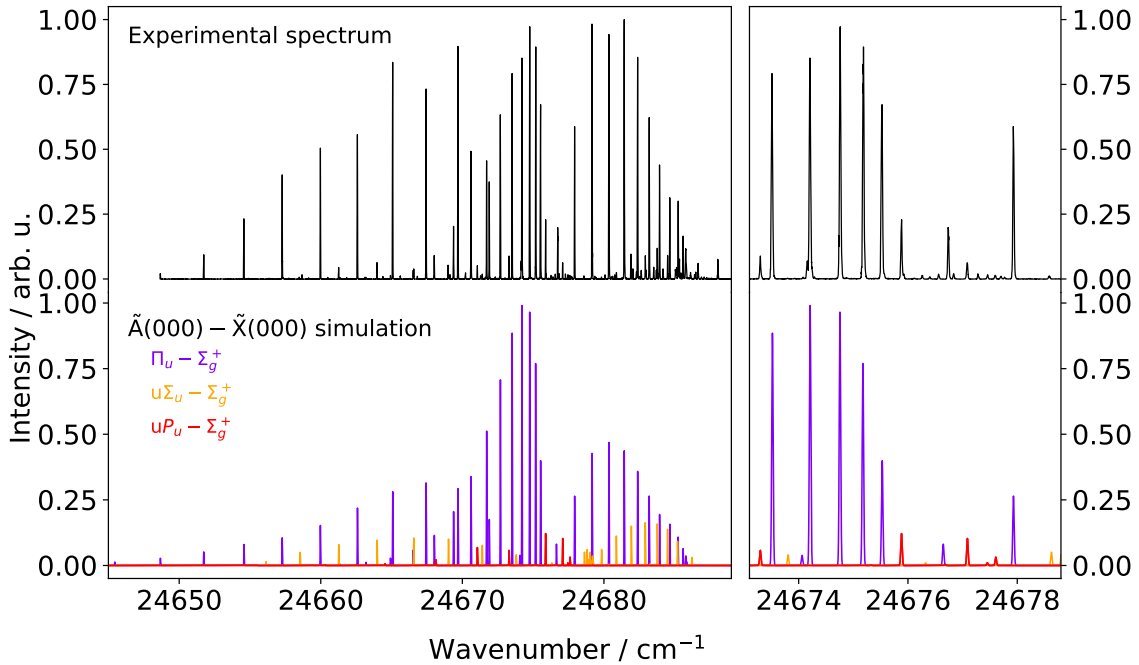


Figure S6: Overview of the $\tilde{A}(000) - \tilde{X}(000)$ band system (left panel), zoom of a portion of the spectral range (right panel) and comparison with a PGOPHER simulation at 70 K (lower traces).

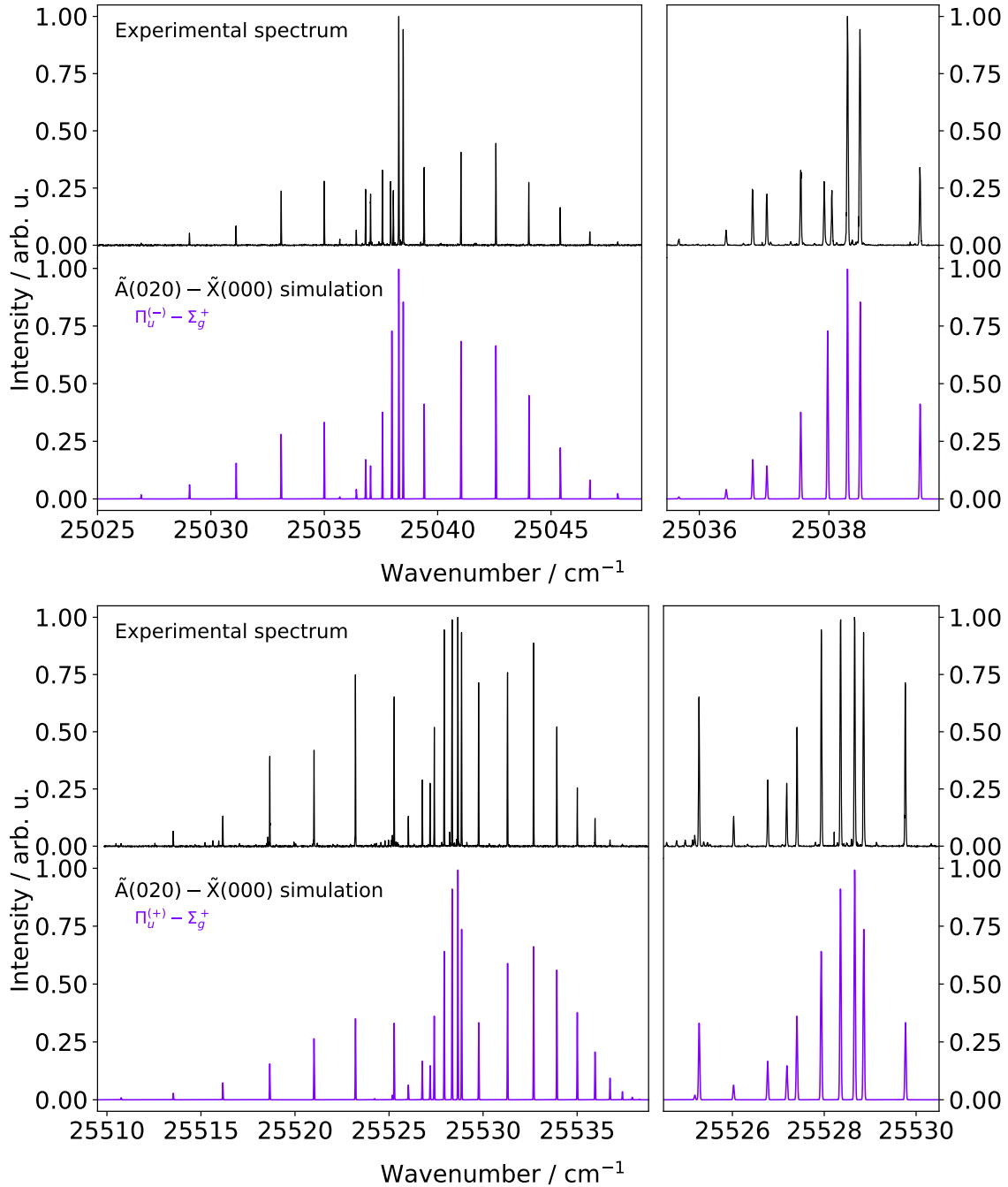


Figure S7: Overview of the $\tilde{A}(020) - \tilde{X}(000)$ band system, $\Pi_u^{(-)} - \Sigma_g^+$ (top panels) and $\Pi_u^{(+)} - \Sigma_g^+$ (lower panels) bands. Full band (left panels) and zoom of a portion of the spectral range (right panels). Comparisons with PGOPHER simulations at 20 K and 30 K, respectively (lower traces).

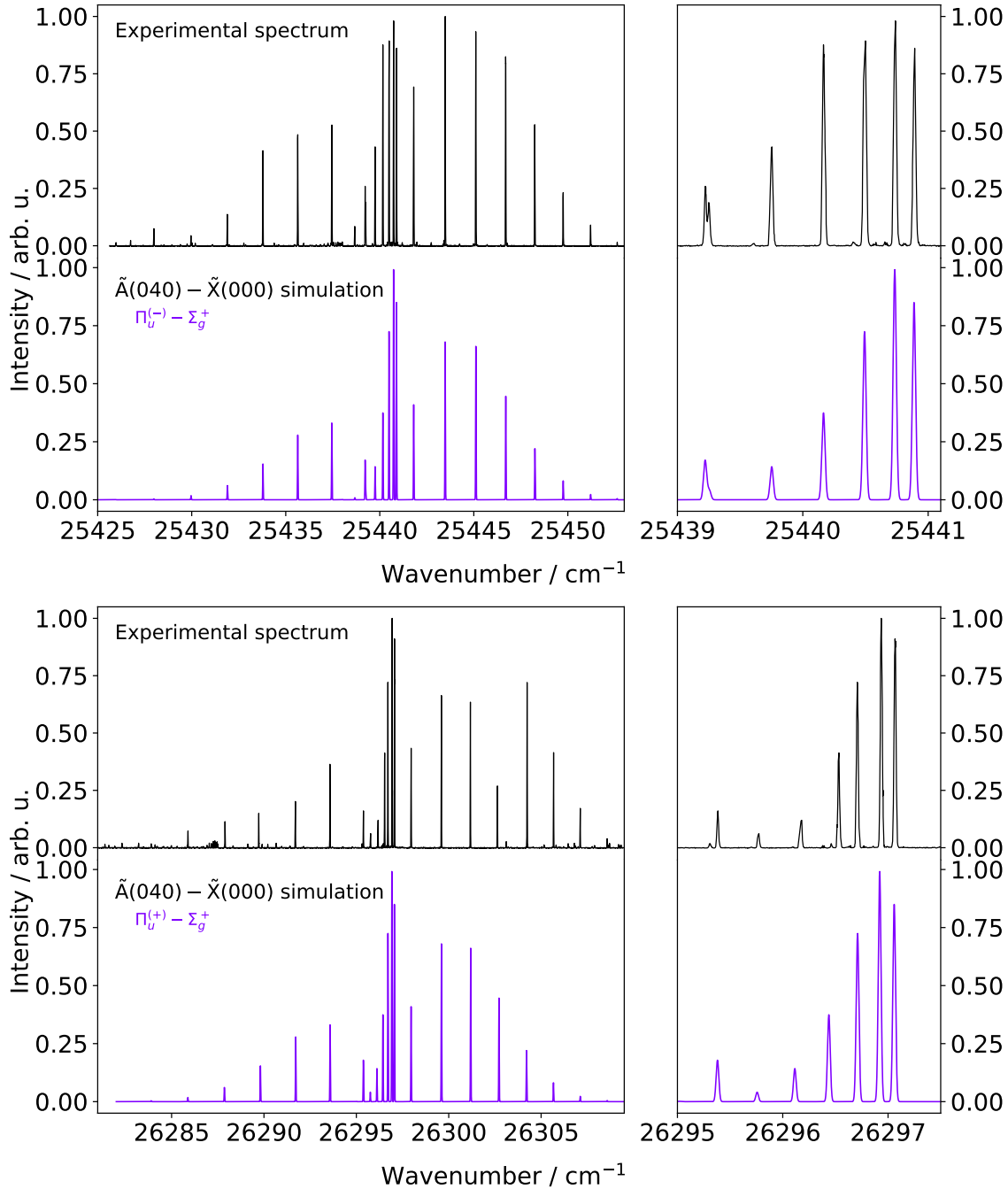


Figure S8: Overview of the $\tilde{A}(040) - \tilde{X}(000)$ band system, $\Pi_u^{(-)} - \Sigma_g^+$ (top panels) and $\Pi_u^{(+)} - \Sigma_g^+$ (lower panels) bands. Full band (left panels) and zoom of a portion of the spectral range (right panels). Comparisons with PGOPHER simulations at 20 K (lower traces).

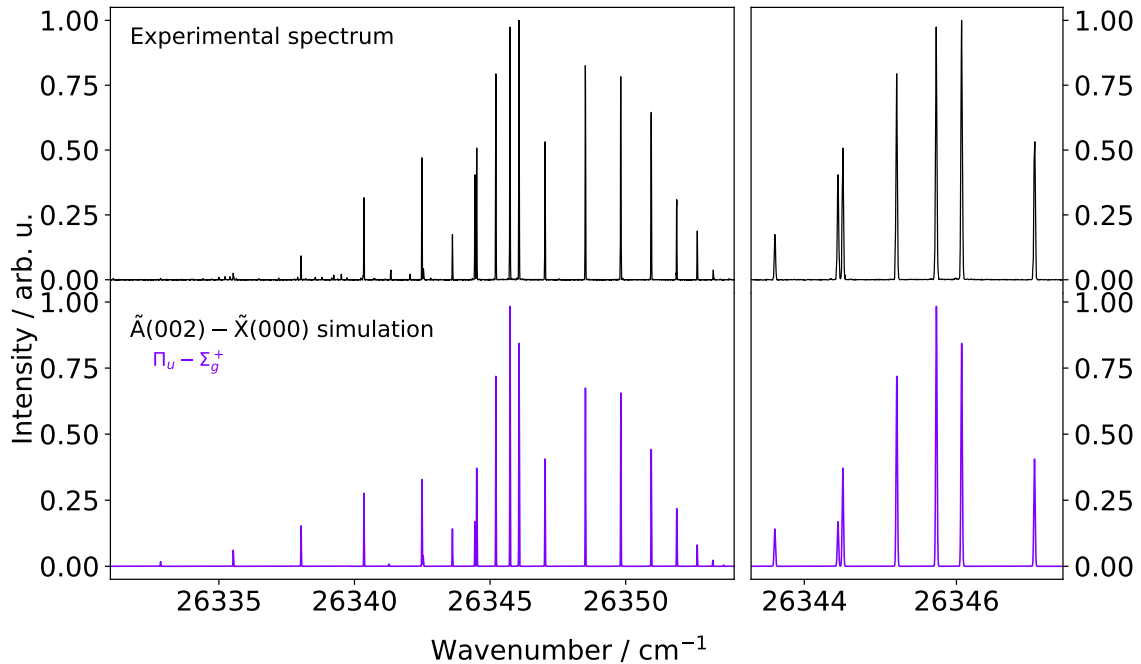


Figure S9: Overview of the $\tilde{A}(002) - \tilde{X}(000)$ band (left panel), zoom of a portion of the spectral range (right panel), and comparison with a PGOPHER simulation at 20 K (lower traces).

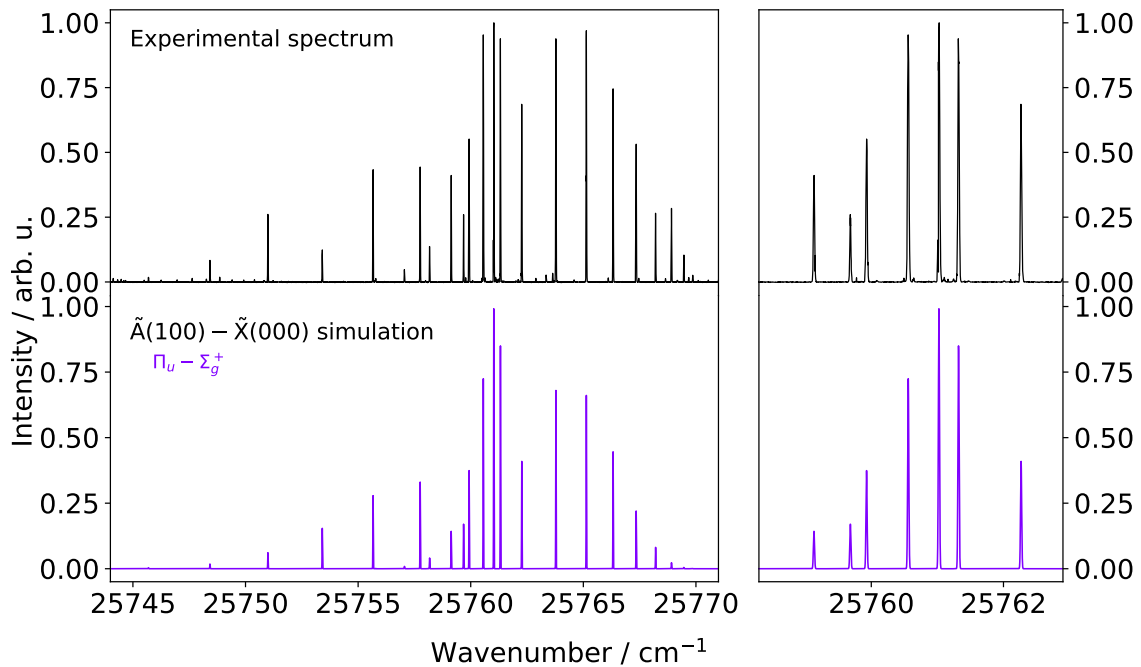


Figure S10: Overview of the $\tilde{A}(100) - \tilde{X}(000)$ band (left panel), zoom of a portion of the spectral range (right panel), and comparison with a PGOPHER simulation at 20 K (lower traces).

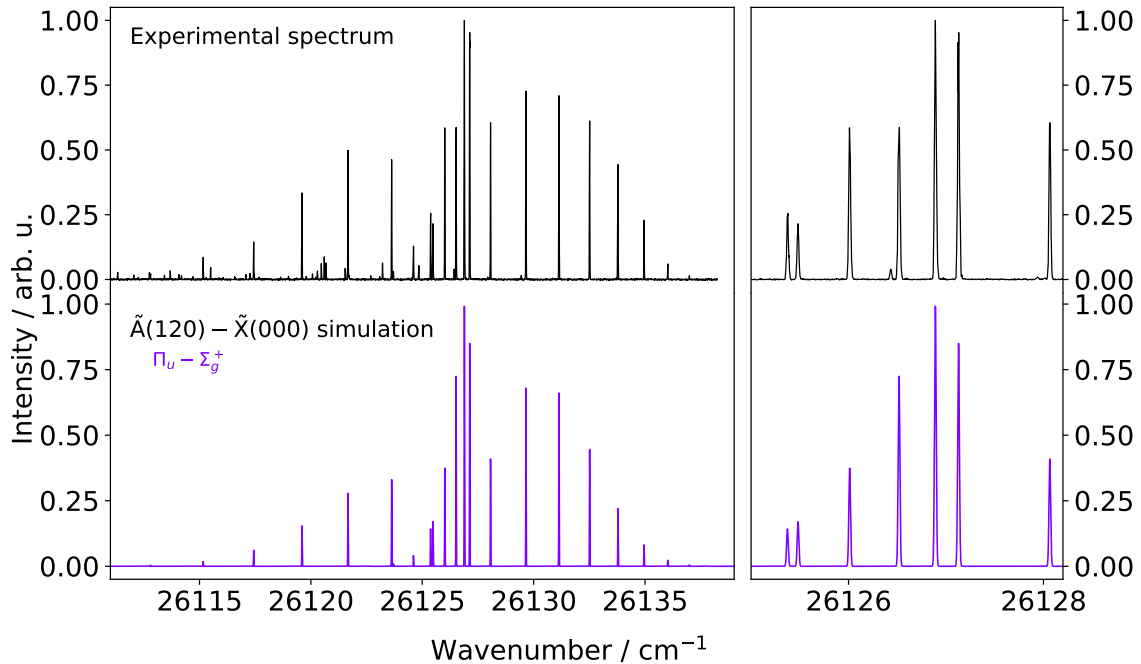


Figure S11: Overview of the $\tilde{A}(120) - \tilde{X}(000)$ band (left panel), zoom of a portion of the spectral range (right panel), and comparison with a PGOPHER simulation at 20 K (lower traces).

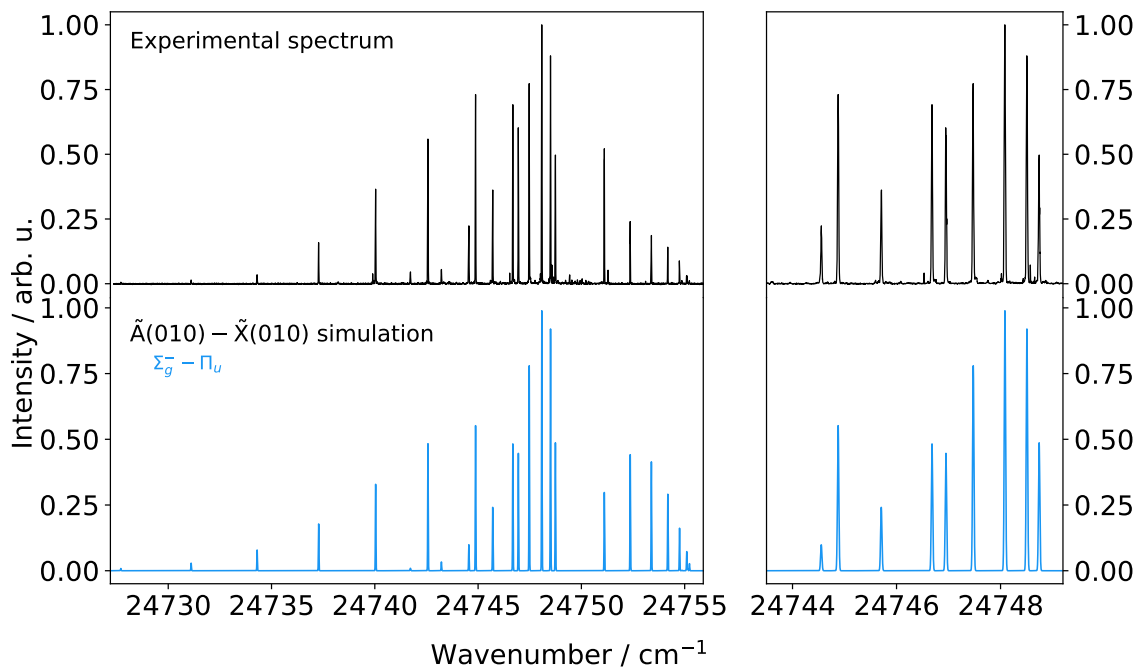


Figure S12: Overview of the $\tilde{A}(010) - \tilde{X}(010)$ $\Sigma_g^- - \Pi_u$ band (left panel), zoom of a portion of the spectral range (right panel), and comparison with a PGOPHER simulation at 30 K (lower traces).

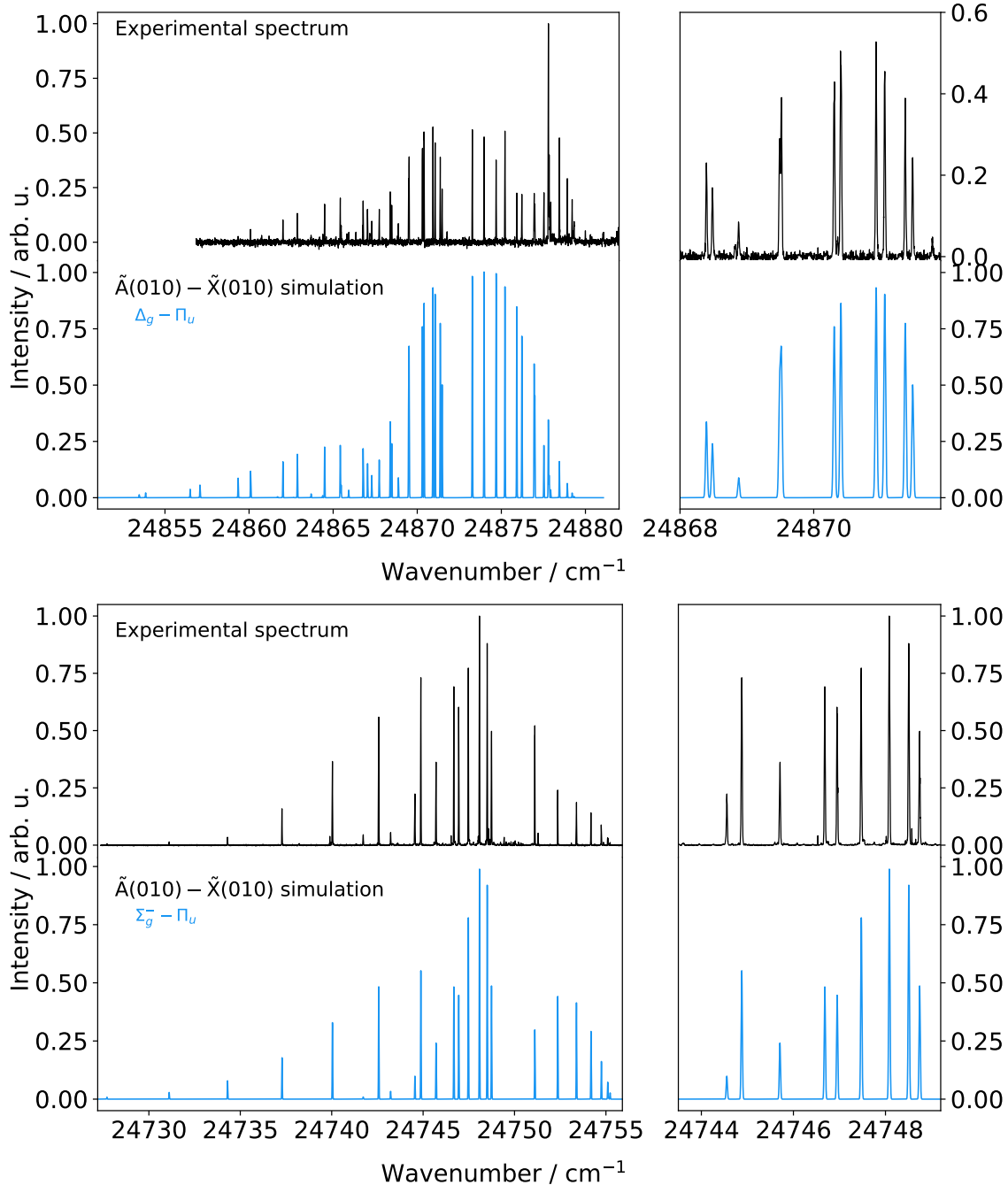


Figure S13: Overview of the $\tilde{A}(010) - \tilde{X}(010)$ $\Delta_g - \Pi_u$ (top panels) and $\Sigma_g^+ - \Pi_u$ (lower panels) bands. Full band (left panels) and zoom of a portion of the spectral range (right panels). Comparisons with PGOPHER simulations at 30 K (lower traces).

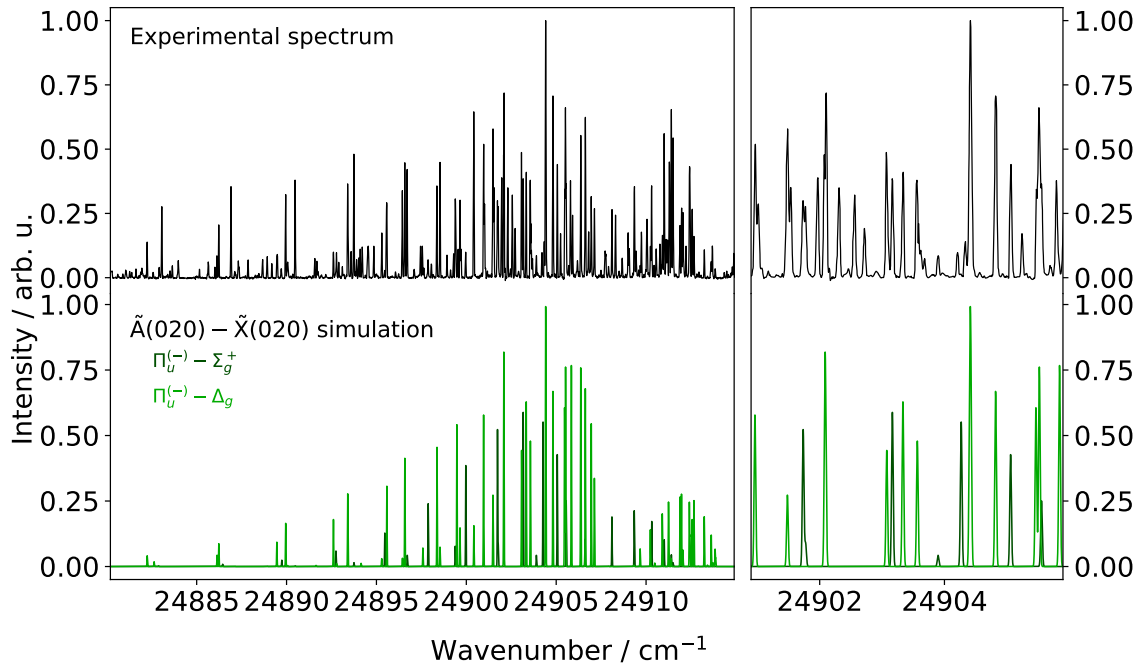


Figure S14: Overview of the $\tilde{A}(020) - \tilde{X}(020)$ $\Pi_u^{(-)} - \Sigma_g^+$ and $\Pi_u^{(-)} - \Delta_g$ bands (left panel), zoom of a portion of the spectral range (right panel), and comparison with a PGOPHER simulation at 50 K (lower traces).

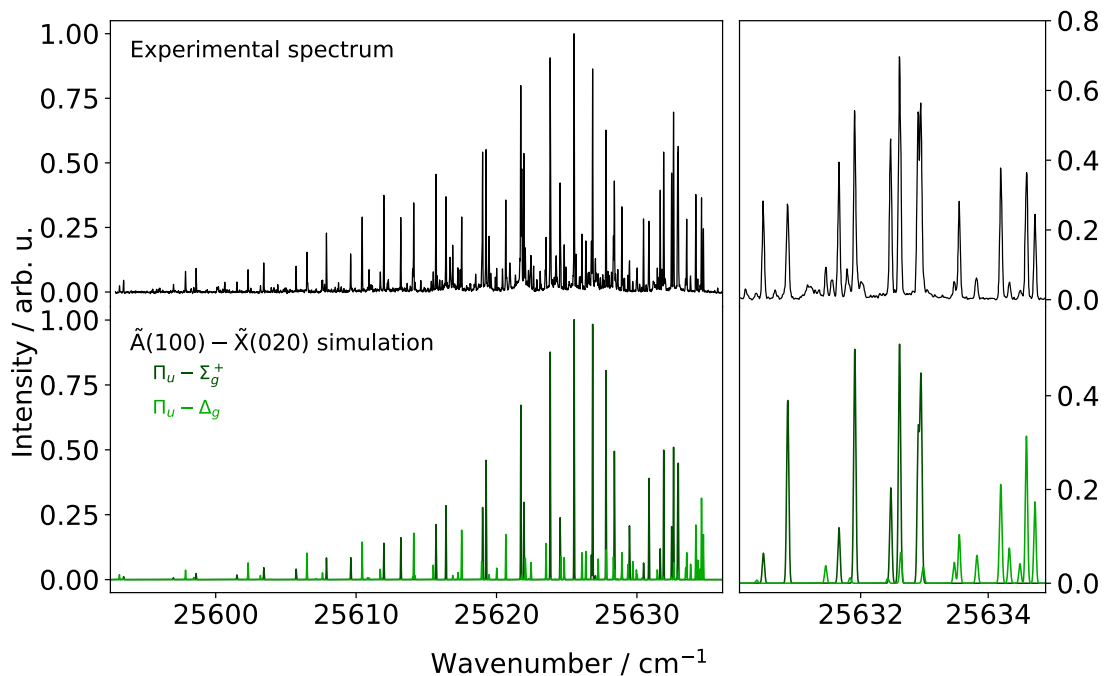


Figure S15: Overview of the $\tilde{A}(100) - \tilde{X}(020)$ $\Pi_u - \Sigma_g^+$ and $\Pi_u - \Delta_g$ bands (left panel), zoom of a portion of the spectral range (right panel), and comparison with a PGOPHER simulation at 70 K (lower traces).

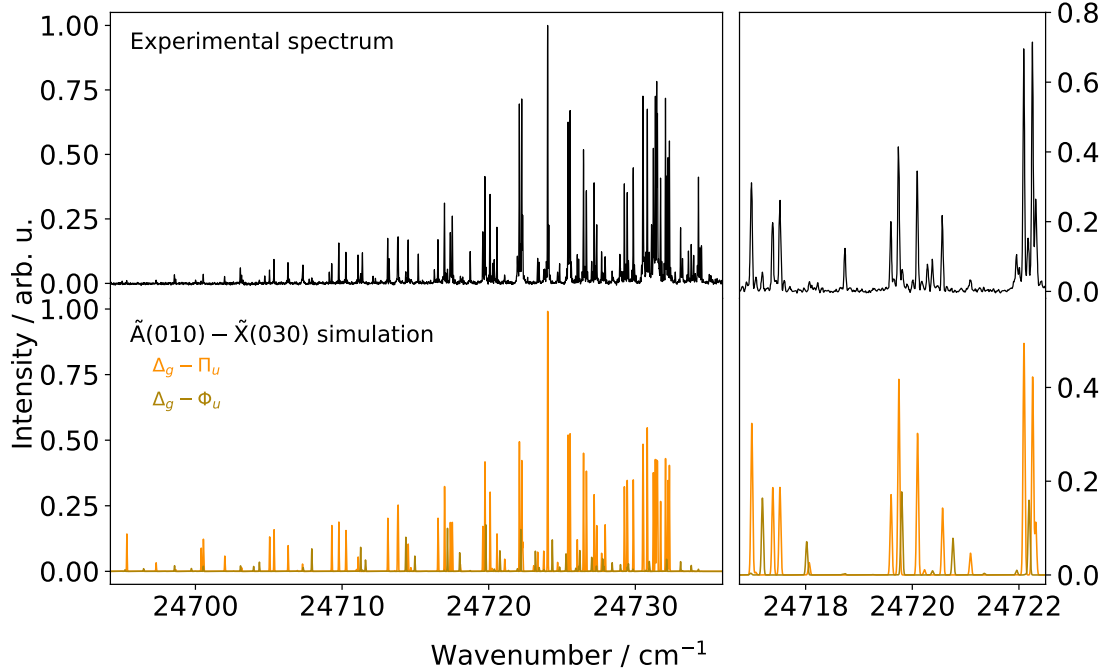


Figure S16: Overview of the $\tilde{A}(010) - \tilde{X}(030)$ $\Delta_g-\Pi_u$ and $\Delta_g-\Phi_u$ bands (left panel), zoom of a portion of the spectral range (right panel), and comparison with a PGOPHER simulation at 100 K (lower traces).

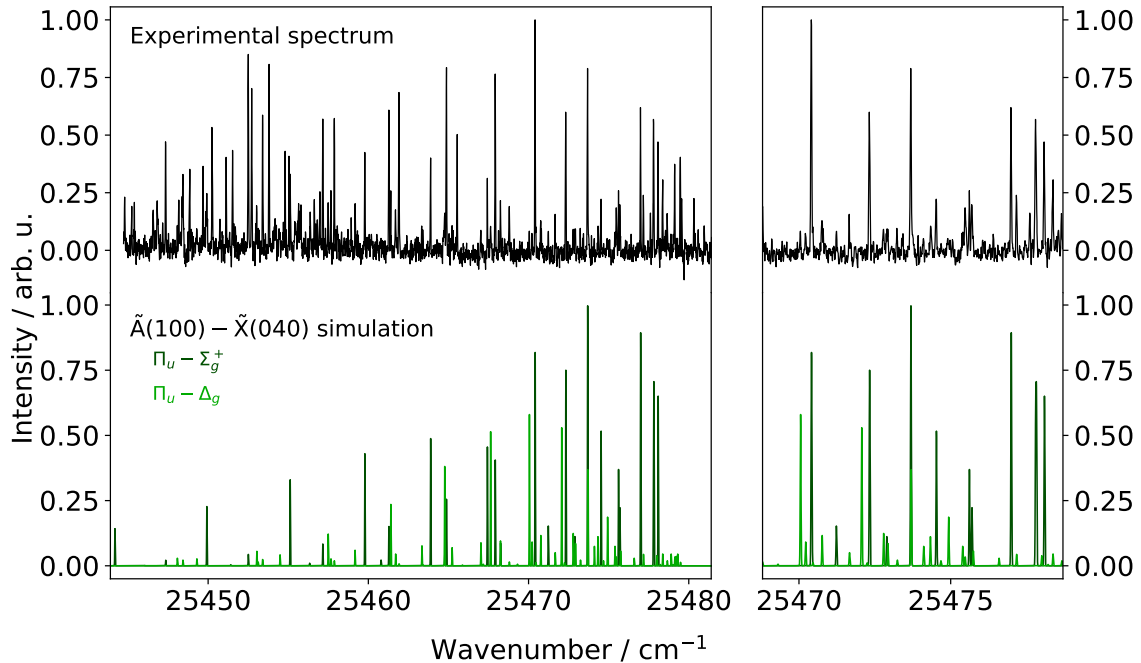


Figure S17: Overview of the $\tilde{A}(100) - \tilde{X}(040)$ $\Pi_u-\Sigma_g^+$ and $\Pi_u-\Delta_g$ bands (left panel), zoom of a portion of the spectral range (right panel), and comparison with a PGOPHER simulation at 70 K (lower traces).

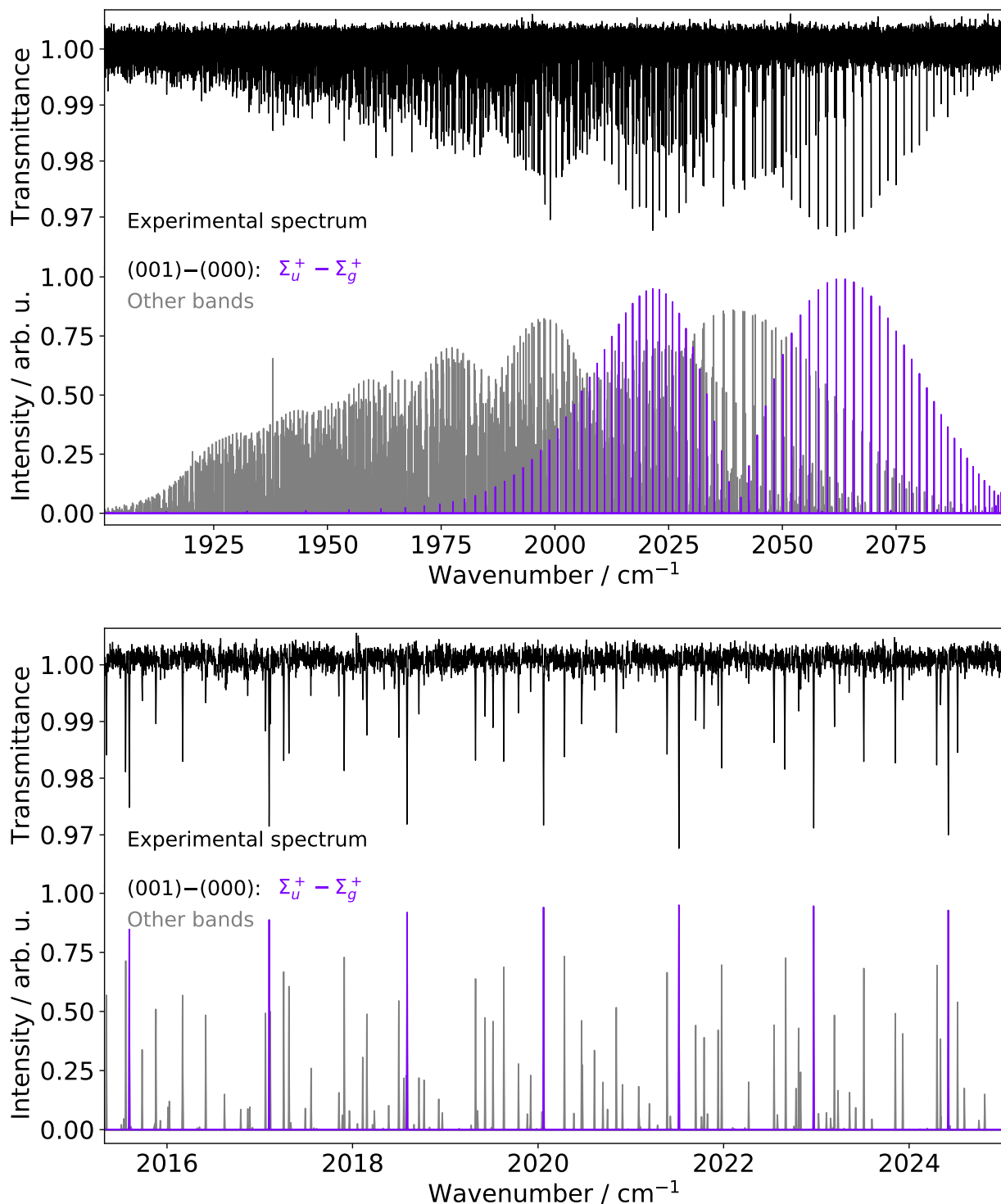


Figure S18: Overview of the (001)–(000) band (top panel) and zoom of the P-branch (lower panel). *Top trace:* experimental spectrum, in transmittance, after removal of CO, H₂O, and C₂H lines. *Bottom trace:* PGOPHER simulations at 500 K (final set of parameters), in gray, with the (001)–(000) band highlighted in purple.

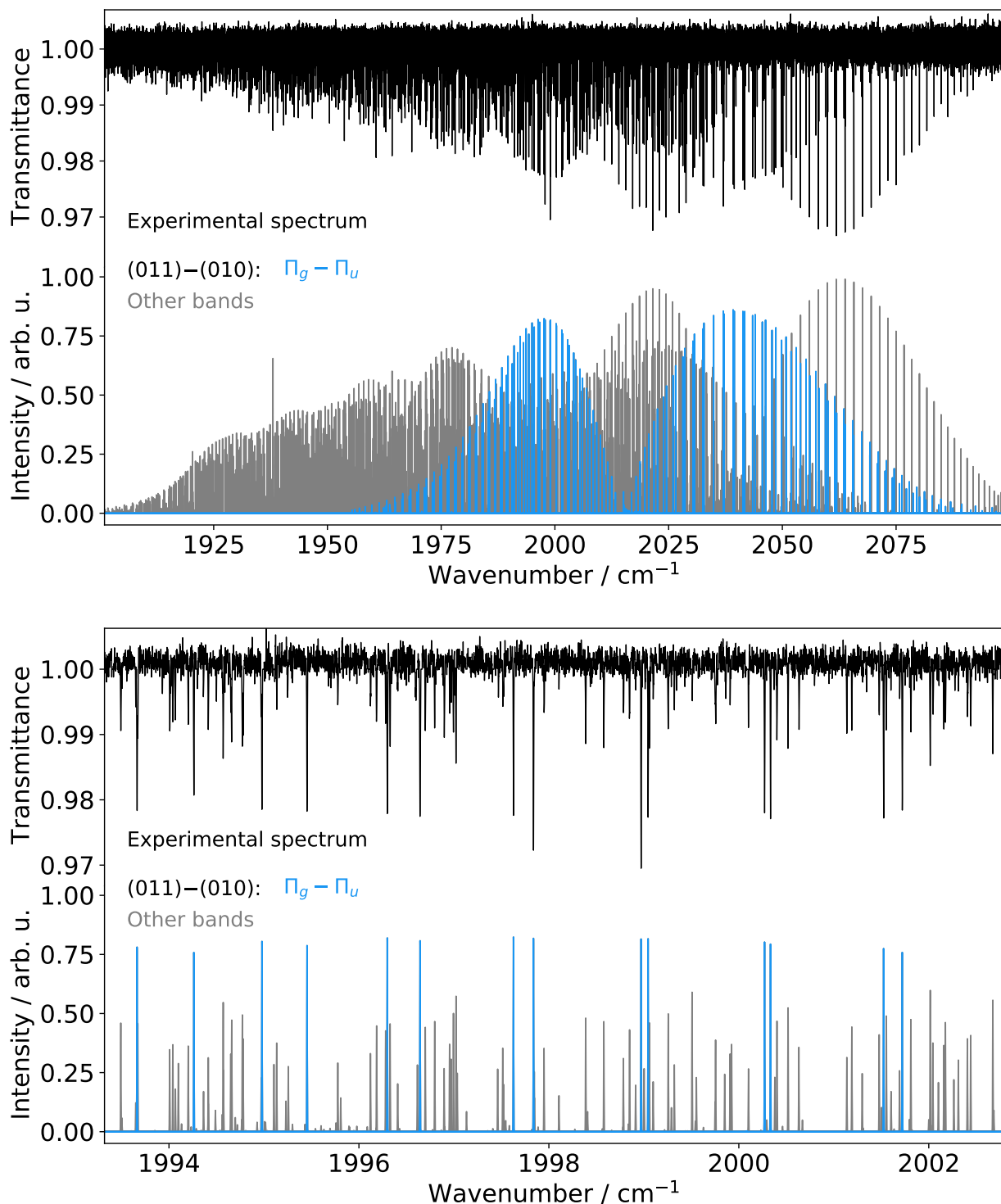


Figure S19: Overview of the (011)–(010) band (top panel) and zoom of the P-branch (lower panel). *Top trace:* experimental spectrum, in transmittance, after removal of CO, H₂O, and C₂H lines. *Bottom trace:* PGOPHER simulations at 500 K (final set of parameters), in gray, with the (011)–(010) band highlighted in blue.

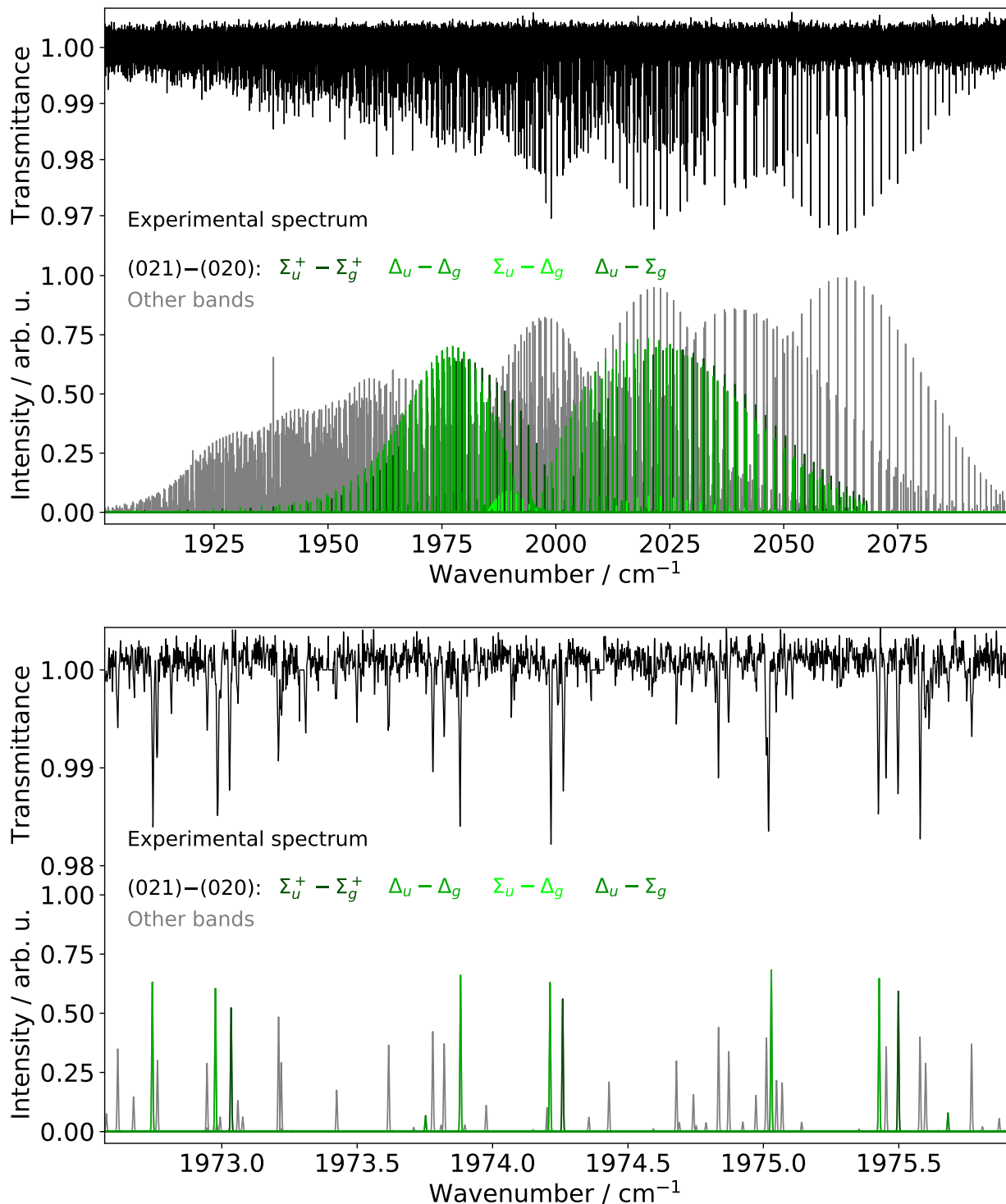


Figure S20: Overview of the (021)–(020) infrared bands (top panel) and zoom of the P-branches (lower panel). *Top trace:* experimental spectrum, in transmittance, after removal of CO, H₂O, and C₂H lines. *Bottom trace:* PGOPHER simulations at 500 K (final set of parameters), in gray, with the (021)–(020) bands highlighted in shades of green.

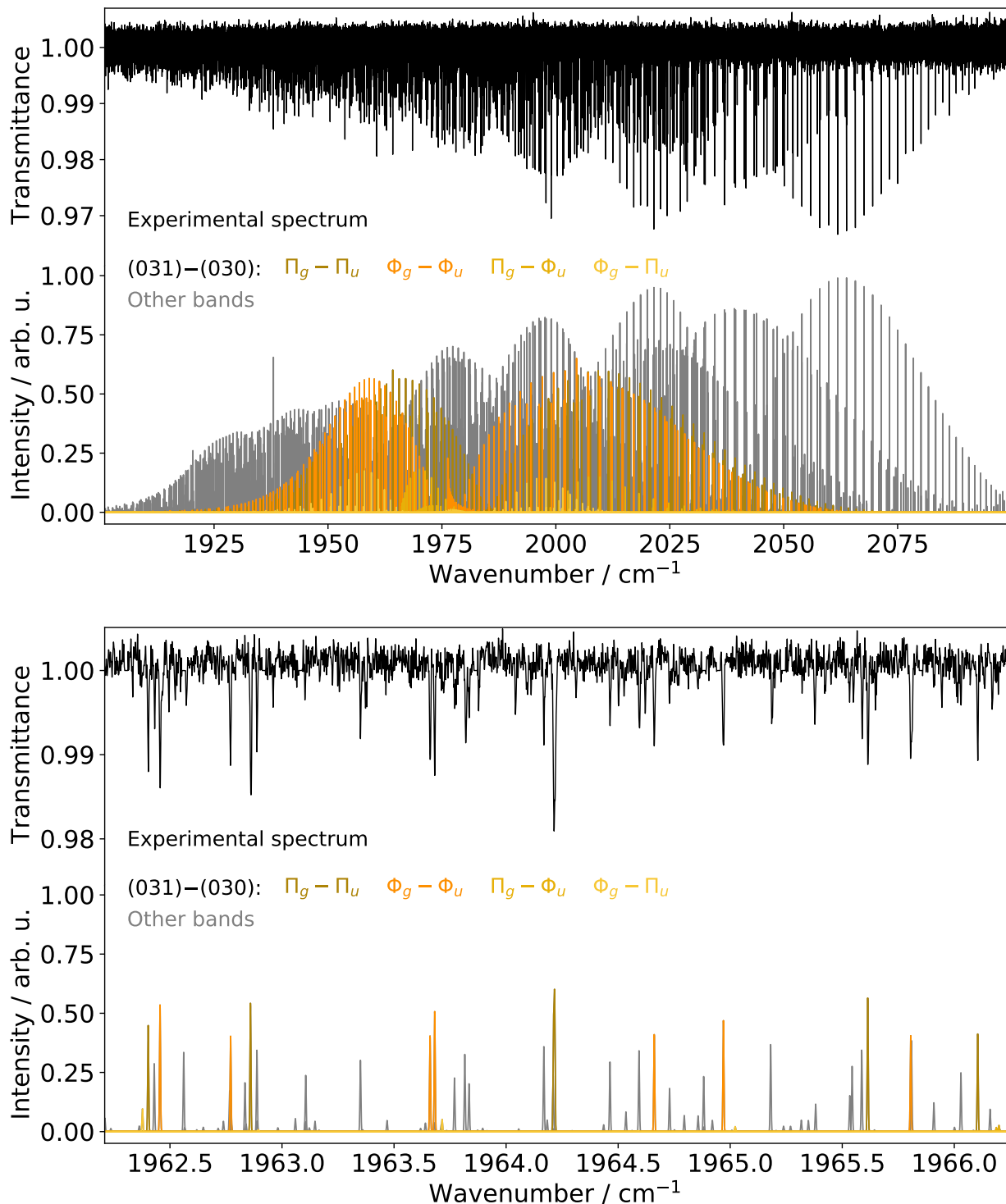


Figure S21: Overview of the (031)–(030) infrared bands (top panel) and zoom of the P-branches (lower panel). *Top trace:* experimental spectrum, in transmittance, after removal of CO, H₂O, and C₂H lines. *Bottom trace:* PGOPHER simulations at 500 K (final set of parameters), in gray, with the (031)–(030) bands highlighted in shades of yellow.

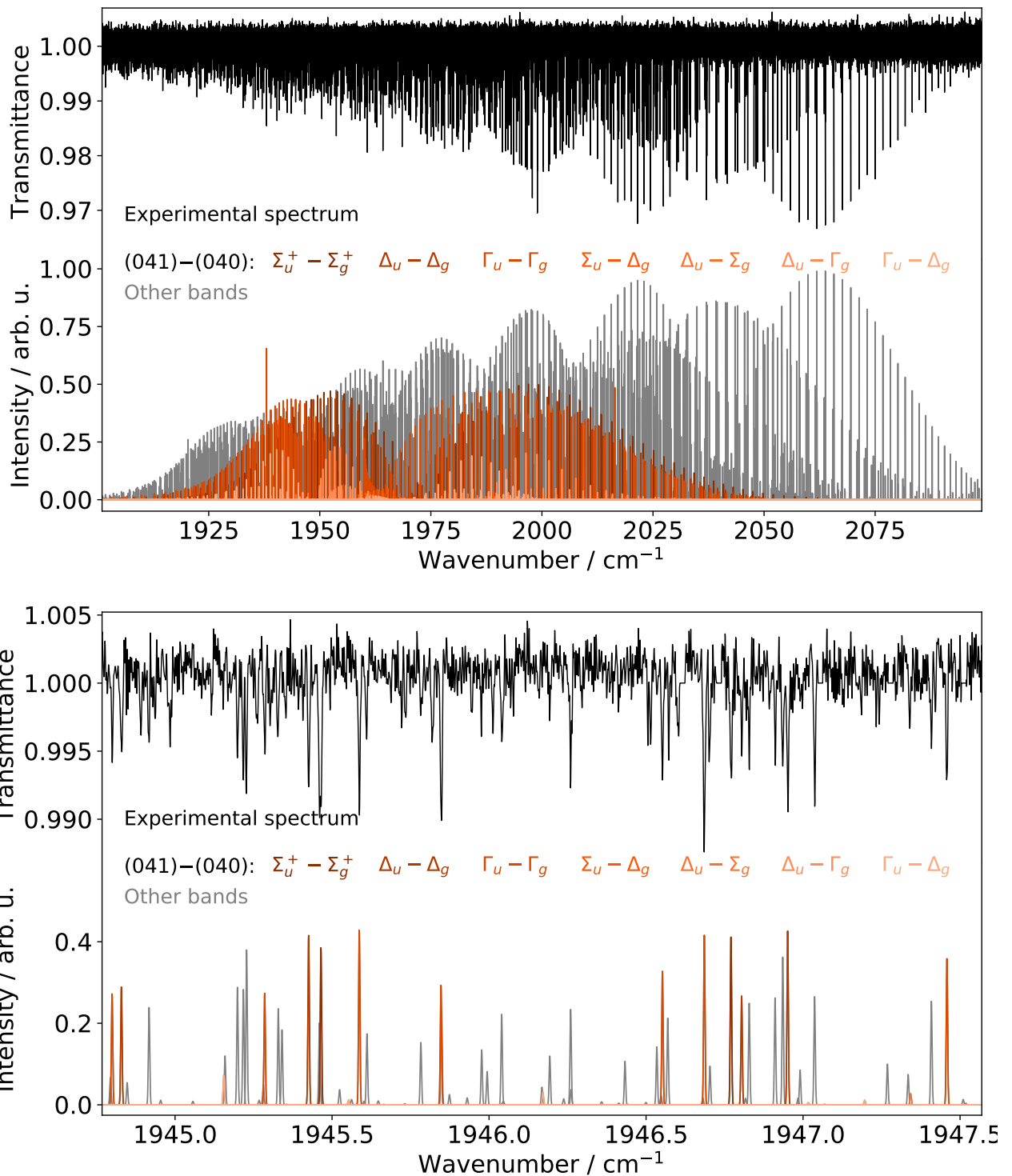


Figure S22: Overview of the (041)–(040) infrared bands (top panel) and zoom of the P-branches (lower panel). *Top trace:* experimental spectrum, in transmittance, after removal of CO, H₂O, and C₂H lines. *Bottom trace:* PGOPHER simulations at 500 K (final set of parameters), in gray, with the (041)–(040) bands highlighted in shades of orange.

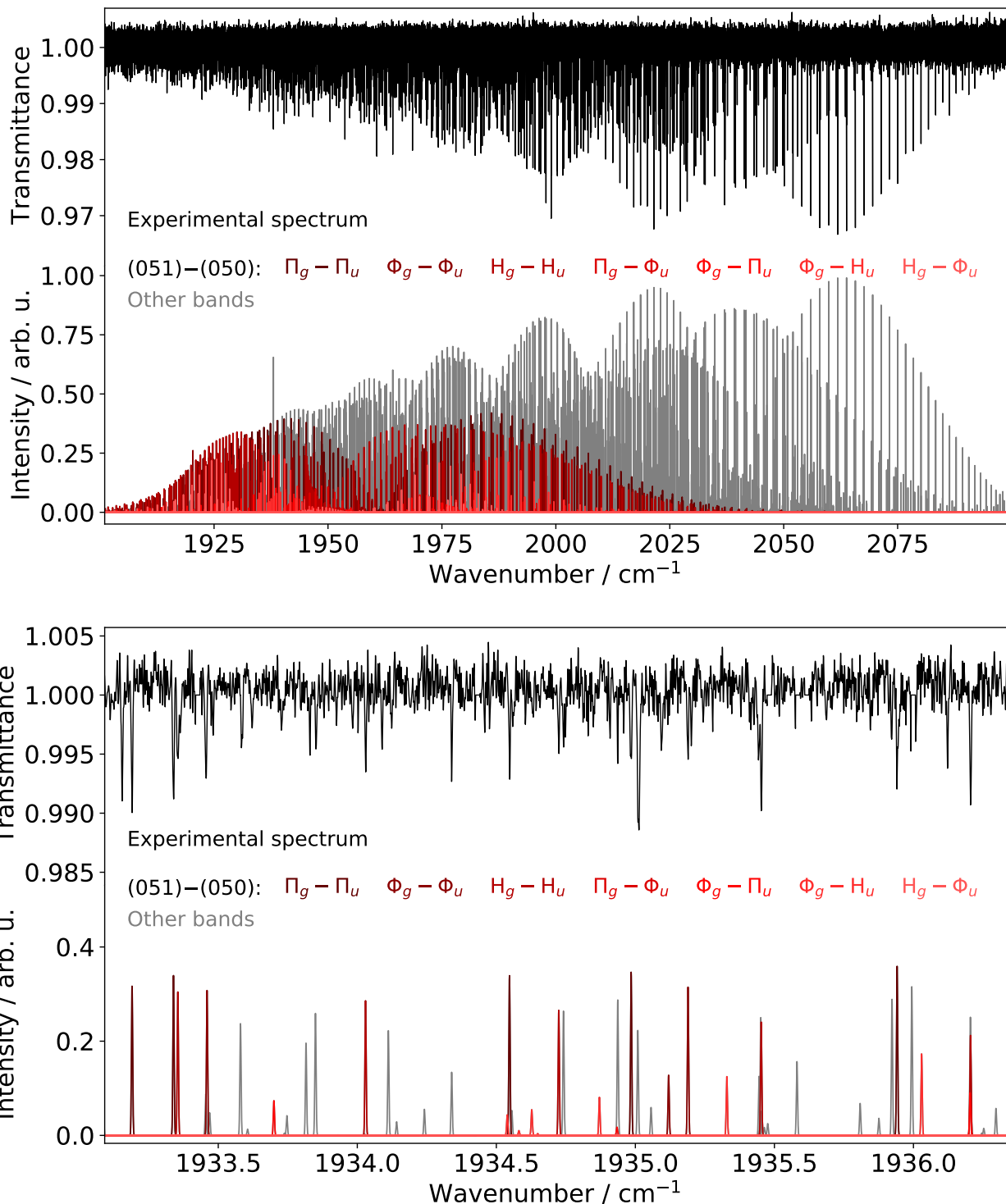


Figure S23: Overview of the (051)–(050) infrared bands (top panel) and zoom of the P-branches (lower panel). *Top trace:* experimental spectrum, in transmittance, after removal of CO, H₂O, and C₂H lines. *Bottom trace:* PGOPHER simulations at 500 K (final set of parameters), in gray, with the (051)–(050) bands highlighted in shades of red.

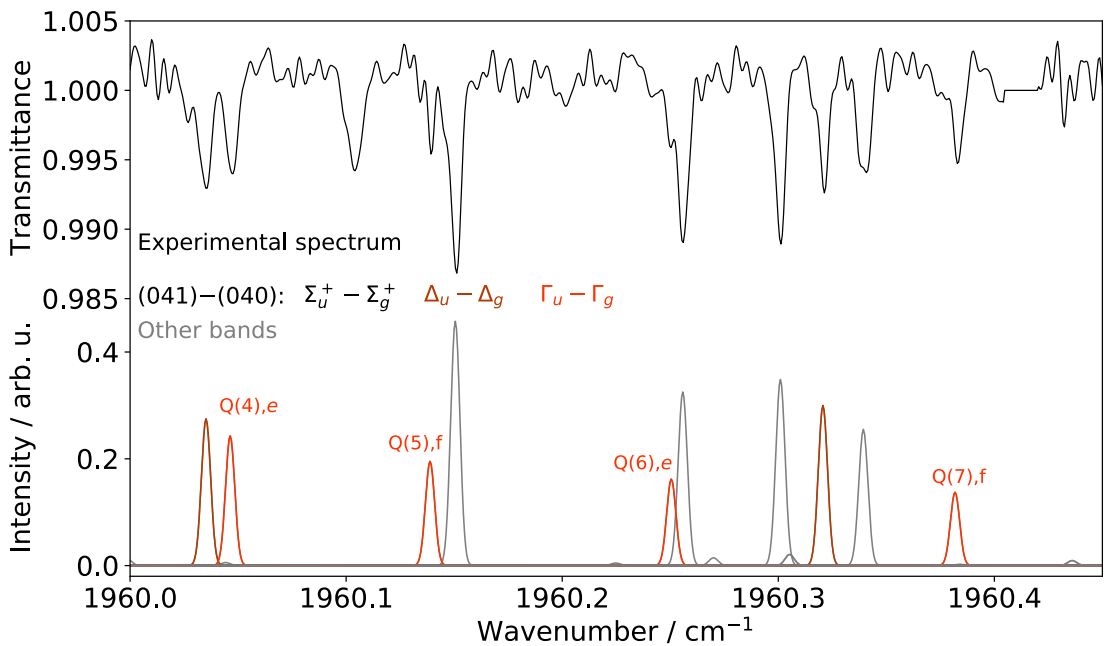


Figure S24: zoom of the Q-branch of the $(041)-(040)$ $\Gamma_u - \Gamma_g$ infrared band. *Top trace:* experimental spectrum, in transmittance, after removal of CO, H₂O, and C₂H lines. *Bottom trace:* PGOPHER simulations at 700 K (final set of parameters).

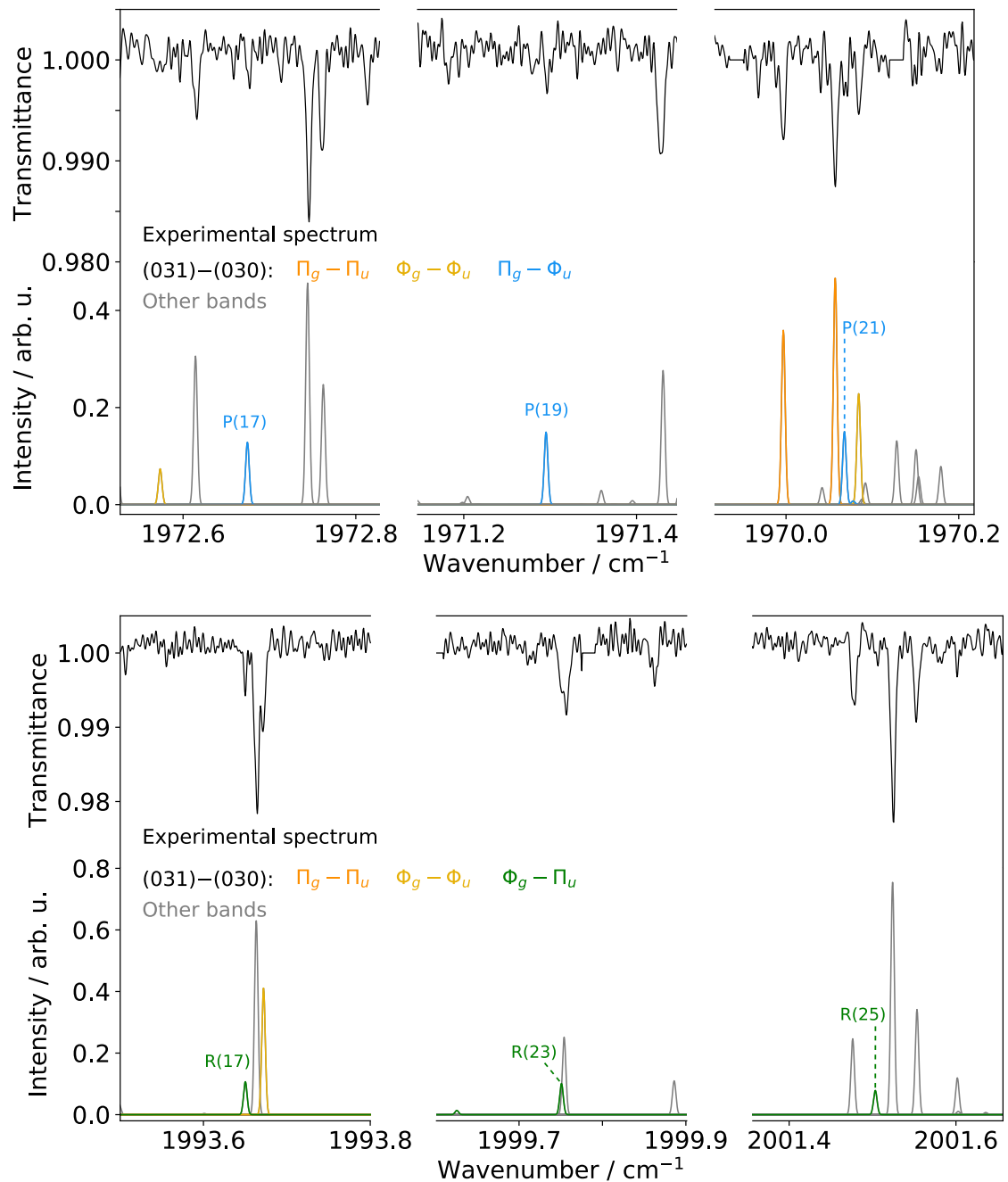


Figure S25: Zoom of three P-branch transitions of the $(031)-(030)$ $\Pi_g-\Phi_u$ (upper panel) and R-branch transitions of the the $\Phi_g-\Pi_u$ bands (lower panel). *Top traces:* experimental spectrum, in transmittance, after removal of CO, H₂O, and C₂H lines. *Bottom traces:* PGOPHER simulations at 700 K (final set of parameters, normalized to the strongest transition of the fundamental ν_3 band) where the $\Pi_g-\Phi_u$ and $\Phi_g-\Pi_u$ transitions are highlighted in blue and green, respectively. The rest of the simulated transitions of the $(031)-(030)$ bands visible in this range are plotted in shades of orange while the others C₃ bands are simulated in gray.

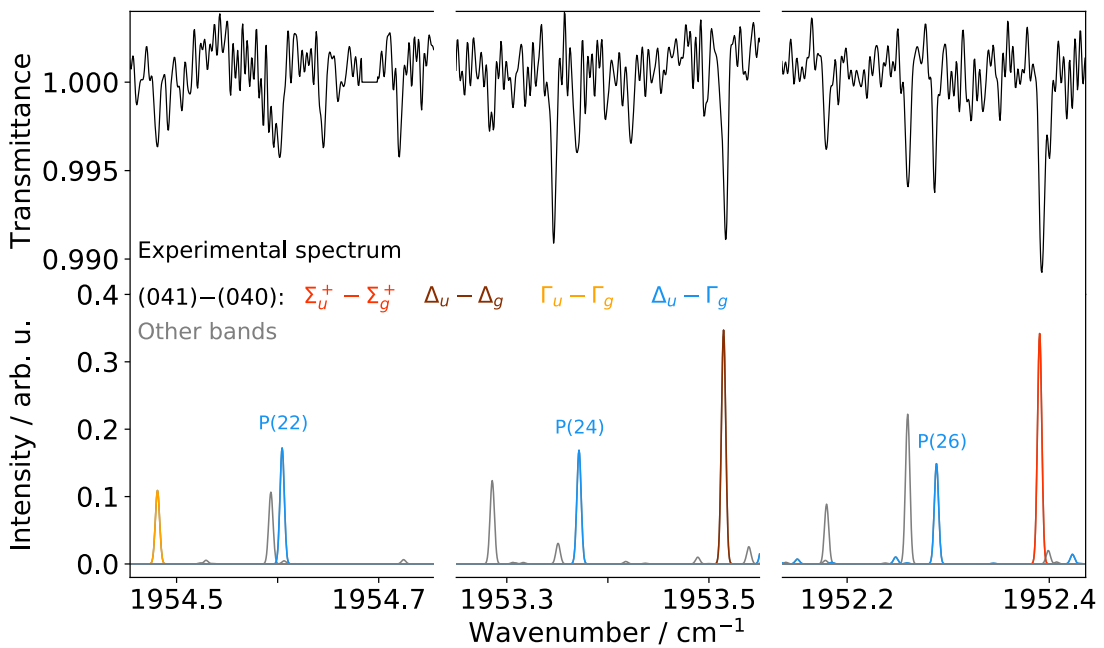


Figure S26: Zoom of three consecutive P-branch transitions of the (041)–(040) $\Delta_u - \Gamma_g$ band. *Top trace:* experimental spectrum, in transmittance, after removal of CO, H₂O, and C₂H lines. *Bottom trace:* PGOPHER simulations at 700 K (final set of parameters, normalized to the strongest transition of the fundamental ν_3 band) where the $\Delta_u - \Gamma_g$ transitions are highlighted in blue. The rest of the simulated transitions of the (041)–(040) bands visible in this range are plotted in shades of red while the others C₃ bands are simulated in gray.

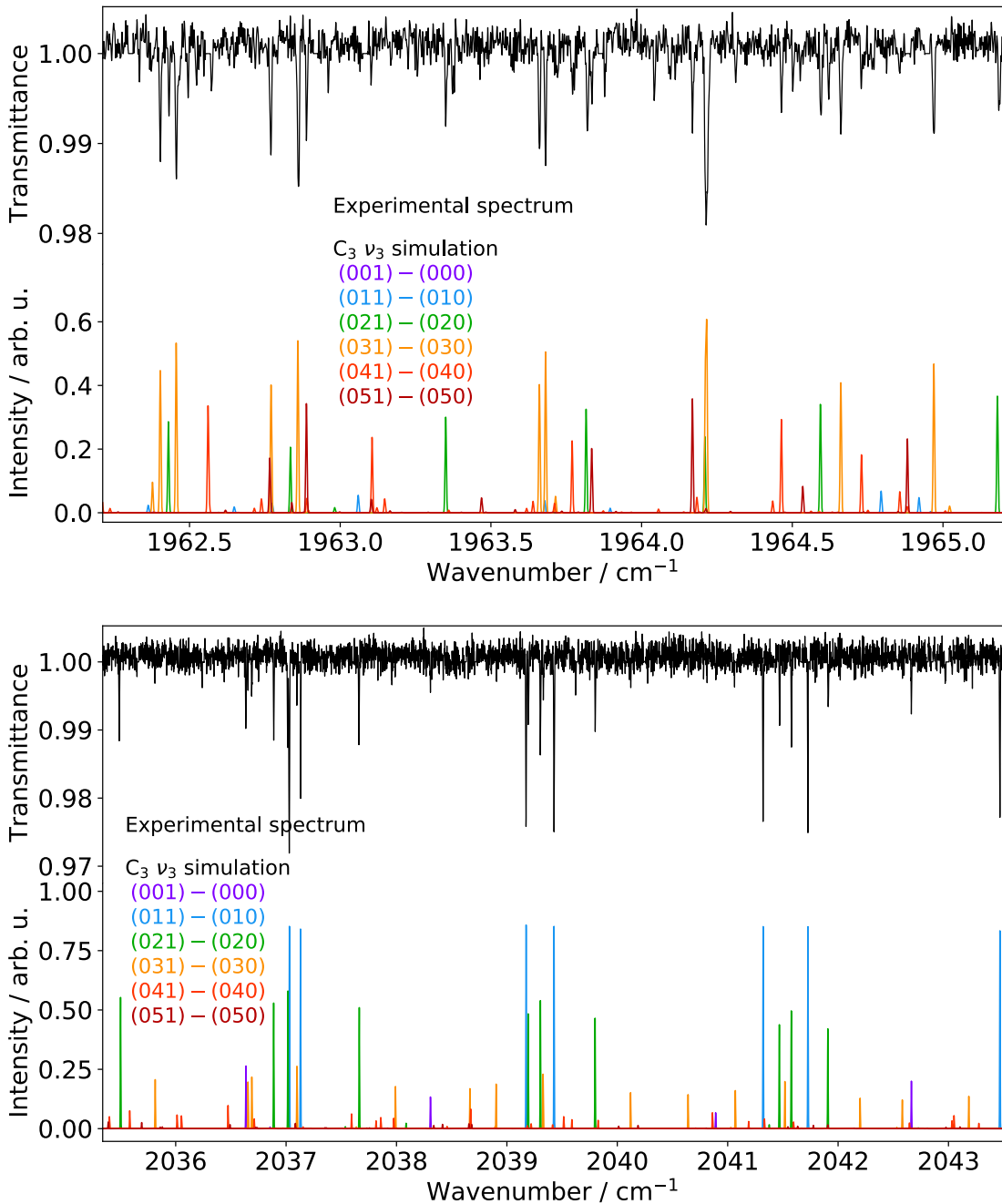
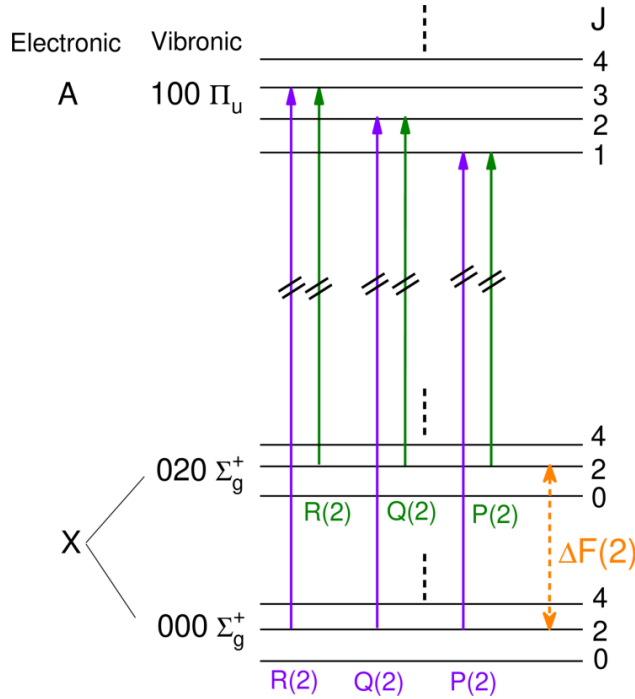


Figure S27: Zoom of portions of the infrared spectrum. *Top trace:* experimental spectrum, in transmittance, after removal of CO, H₂O, and C₂H lines. *Bottom trace:* PGOPHER simulations at 700 K (final set of parameters, normalized to the strongest transition of the fundamental ν_3 band). The hot band sequence is plotted in a color sequence ranging from purple to dark red.

3 Analysis of the infrared spectrum: Determination of bend rovibrational energies

To enable the assignment of the rovibrational data, the bending rovibrational energies were first determined from the line positions of hot bands in combination with appropriate fundamental bands. Here, the determination of the $\tilde{X}(020) \Sigma_g^+$ rovibrational energy levels is given as an example illustrating the basic idea of this procedure. The figure below schematically draws several transitions of $\tilde{A}(100)-\tilde{X}(000)$ and $\tilde{A}(100)-\tilde{X}(020) \Pi_u-\Sigma_g^+$ bands. It can be seen that the two R(2) lines originate from different rovibrational levels in the ground state (the $J'' = 2$ level of the $\tilde{X}(000) \Sigma_g^+$ state and the $J'' = 2$ level of the $\tilde{X}(020) \Sigma_g^+$ state, respectively) but end at the same rovibrational level in the excited state (the $J' = 3$ level of the $\tilde{A}(100) \Sigma_g^+$ state). The difference in energy of these two R(2) transitions is the “fictitious transition” between the $\tilde{X}(000)$ and $\tilde{X}(020) \Sigma_g^+$ states for $J'' = 2$ and denoted as $\Delta F(2)$ (as shown in the figure below). A similar analysis can be carried out for the two Q(2) and two P(2) transitions to also determine $\Delta F(2)$, and an average of which is used for statistical accuracy. Since the rovibrational energy of the $J'' = 2$ level of the $\tilde{X}(000)$ state, denoted as $F_{000}(2)$, is available from [Schmuttenmaer et al. \[1990\]](#) and [Gendriesch et al. \[2003\]](#), then the $J'' = 2$ rotational level energy of the $\tilde{X}(020) \Sigma_g^+$ state, denoted $F_{020}(2)$, can be calculated from:

$$F_{020}(2) = \Delta F(2) + F_{000}(2)$$



Schematic energy level diagram of the $\tilde{A}(100) \Pi_u$, $\tilde{X}(020) \Sigma_g^+$, and $\tilde{X}(000) \Sigma_g^+$ allowing to determine the $\tilde{X}(020) \Sigma_g^+$ rovibrational energy levels from combination difference. R(2), Q(2) and P(2) transitions are displayed with purple and green arrows for the $\tilde{A}(100)-\tilde{X}(000) \Pi_u-\Sigma_g^+$ and $\tilde{A}(100)-\tilde{X}(020) \Pi_u-\Sigma_g^+$ bands, respectively.

This procedure is repeated for all J'' levels that have observed transitions in both $\tilde{A}(100)-\tilde{X}(020) \Pi_u-\Sigma_g^+$ and $\tilde{A}(100)-\tilde{X}(000) \Pi_u-\Sigma_g^+$ bands, and consequently, the rotational level energies in $\tilde{X}(020) \Sigma_g^+$ vibrionic state can be derived from the experimental data. Besides, the $\tilde{A}(020)-\tilde{X}(020) \Pi_u^{(-)}-\Sigma_g^+$ and $\tilde{A}(020)-\tilde{X}(000) \Pi_u^{(-)}-\Sigma_g^+$ band pairs have been recorded and used to determine the rotational

level energies of $\tilde{X}(020) \Sigma_g^+$. In this way, the rotational assignments of the hot bands and rotational level energies are further confirmed.

The same analysis procedure has been applied to the other hot bands and corresponding reference bands. The resulting rovibrational level energies are summarized in the following table columns 4–8. All these energies are relative to the $\tilde{X}(000)$, $J = 0$ state, which is the rovibrational ground state of C₃. It should be noted that odd- J levels energies in $\tilde{X}(020) \Sigma_g^+$ and $\tilde{X}(040) \Sigma_g^+$ are non-observable due to nuclear spin statistic effects. In addition, columns 2 and 3 present the rovibrational energies of $\tilde{X}(000)$ and $\tilde{X}(010)$ states, which are calculated using the reported spectroscopic constants by [Gendriesch et al. \[2003\]](#).

Determined electronic ground state $\tilde{X}(0v_20)$ Σ_g^+ energy levels of C₃ from combination differences (in cm⁻¹).

J''	(000) Σ_g^+, e				(010) $\Pi_u, e \quad \Pi_u, f$				(020) $\Sigma_g^+, e \quad \Delta_g, e \quad \Delta_g, f$				(030) $\Pi_u, e \quad \Pi_u, f \quad \Phi_u, e \quad \Phi_u f$				(040) $\Sigma_g^+, e \quad \Delta_g, e \quad \Delta_g, f \quad \Gamma_g, e \quad \Gamma_g, f$				(050) $\Pi_u, e \quad \Pi_u, f \quad \Phi_u f \quad H_u, e \quad H_u f$							
0																												
1		63.856				132.789					207.874					286.548					370.882							
2	2.583		65.643	135.502	133.933						209.753					289.367	288.147				372.863							
3		68.252										136.652	212.423					290.959				375.591	373.464					
4	8.611		71.875	141.831	140.273							144.812	220.622		213.476		295.940	294.692				379.627		377.268				
5		76.162											226.523	223.655				299.403				384.031	382.034					
6	18.081		81.667	151.790	150.212								306.310	304.938				311.608				390.261	387.744					
7		87.587				156.586	232.475						230.119		237.510		320.505	318.861				396.248	394.391					
8	30.994		95.015	165.392	163.738								240.511		245.797			327.571				404.788		402.013				
9		102.522					171.978	247.982						258.228			338.553	336.341				412.276						
10	47.345		111.916	182.649	180.815								190.977	267.176		265.100			347.306				423.189		420.068			
11		120.967												279.684	276.145		360.427	357.307				432.217	430.531					
12	67.134		132.365	203.574	201.442									213.589	290.086		304.884		370.817				445.502	441.904				
13		142.916													290.086		287.996					461.479	454.306					
14	90.357		156.355	228.159	225.611												386.123	381.641				471.765						
15		168.366													239.805	316.725						398.113						
16	117.010		183.881	256.392	253.321											333.810		415.629	409.278									
17		197.312														269.607	347.098						429.222					
18	147.089		214.935	288.257	284.558													448.936										
19		229.749														302.996												
20	180.591		249.509	323.747	319.336													489.330										
21		265.671																										
22	217.510		287.595																									
23		305.074																										
24	257.843		329.184																									
25		347.951																										

4 PGOPHER file

4.1 Hamiltonian

4.1.1 General definition of the Hamiltonian

There are two ways of setting up the linear molecule Hamiltonian, it can be changed using the `RSquaredH = True` or `False` parameter in the molecule line. This corresponds to writing the rotational kinetic energy in terms of:

- the angular momentum excluding spin, \hat{N} (`RSquaredH = False`)
- the rotational angular momentum of the nuclear framework, \hat{R} (`RSquaredH = True`)

Further info can be found on the PGOPHER [page](#). Even though the IUPAC convention is to use the \hat{N} form, to enable comparison of the constants derived in this study with literature data, we use here the \hat{R} form (`RSquaredH = True`)

It is important to note that this choice affects both the band origin and the rotational constant. The conversion factors can be found in [de Nijls et al. \[2011\]](#), we report in the table below those of importance for this study.

Conversion factors for the spectroscopic constants from the \hat{R} form (used in this work and most of the literature data) to the \hat{N} form (used for instance in [Haddad et al. \[2014\]](#)).

\hat{R} form	\hat{N} form
E	$T + B - D - q/2$
B	$B - 2D - q/2$
D	D

4.1.2 Λ -doubling

Direct coding of q For Π states q and its centrifugal distortion variants can be coded directly. In that case, q corresponds to the difference between the rotational constants for e and f parity states (for $^1\Pi$). Based on the definition used, it is totally possible than we obtain value of q different by a factor of -1 from the values found in the literature.

For Δ states, q can still be coded directly, but the centrifugal distortion terms cannot anymore. In that case, perturbation objects need to be used. For the sake of uniformity, we decide to use perturbation objects for all states, including the Π states.

Perturbation objects The Λ -doubling is treated using the `Luncouple` or `LNuncouple` operators:

- `Luncouple J` rather than `N` is used in the Hamiltonian
- `LNuncouple N` is used in the Hamiltonian

We used the `LNuncouple` operator in the fit.

About the perturbation order, an explanation can be found on the PGOPHER [page](#). For instance, for Δ states a value of $n = 2$ is used $n = 2$ to treat a perturbation between $l = \pm 2$ and $l = 0$ (thus a difference of 2).

It is important to note that there is a $1/2$ scale factor between the parameter reported using the perturbation objects and the actual value of q (or its centrifugal distortion values).

4.1.3 States

We define a manifold per vibronic state, that we thus call $Xv_1v_2v_3$ and $Av_1v_2v_3$, $v_1v_2v_3$ being the number of quanta of excitation in ν_1 , ν_2 , and ν_3 , respectively. We then label each possible state with its symmetry, e.g. Sigma for Σ , Delta for Δ , Phi for Φ , Gamma for Γ , H for H .

An illustration of the structure of the PGOPHER file is displayed in the following figure.

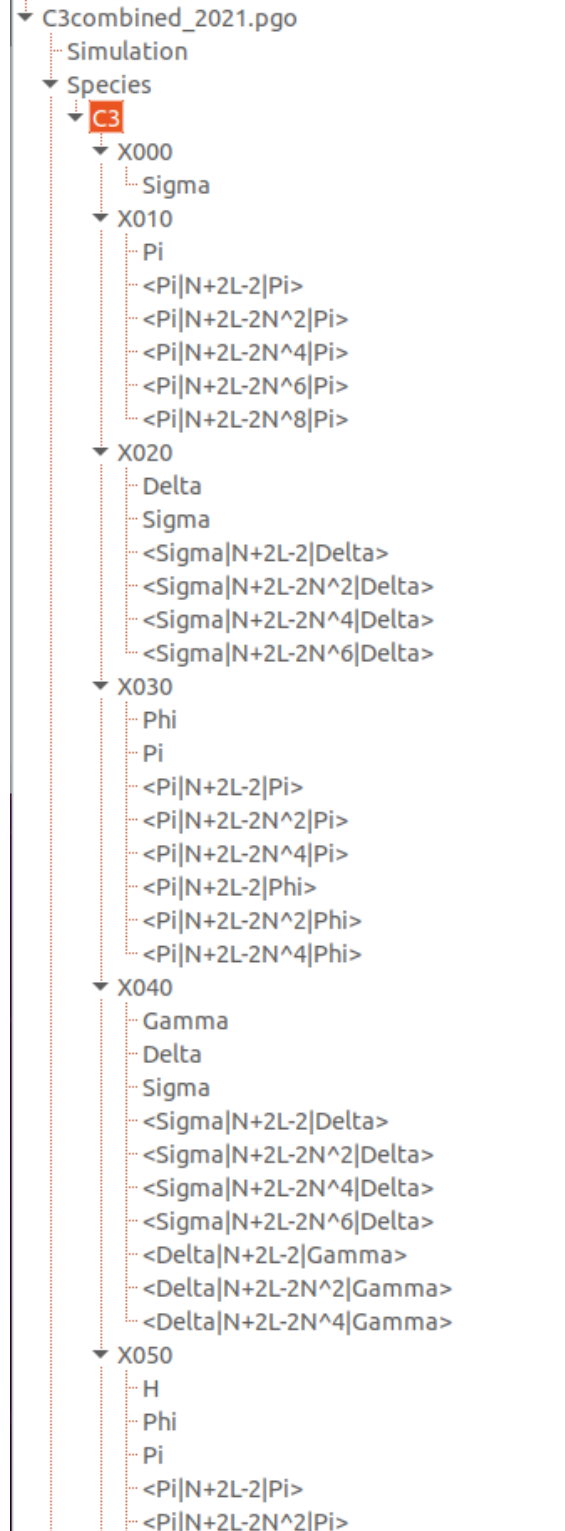


Illustration of the structure of the PGOPHER file

4.2 External linelist files

To manipulate all data more easily, including using several files, we use external ASCII files with assignments instead of a linelist directly in PGOPHER. We follow recommendations from the PGOPHER page and create a master file `master.obs` containing the input commands. We then create one observation file per band. We chose the simplest format for defining each energy level: J and parity (e/f). The Manifolds and states have to be defined for each band and sub-band and the file can contain as many state as desired. Each transitions is then coded as:

`J' p' J'' p'' freq unc : ref`

Example of the `master.obs` file

```
include X010-X000.obs
include X001-X000.obs
include X031-X030.obs
...
```

Example of the `X010-X000.obs` file

```
NQN 2
UpperState X010.Pi
LowerState X000.Sigma

units cm-1

 1 e    2 e    61.26976      2.3E-5   : Schmuttenmaer1990
 3 e    4 e    59.63761      2.3E-5   : Schmuttenmaer1990
...
units MHz

 2 f    2 e    1890558.036    0.250    : Gendrisch2003
 4 f    4 e    1896706.555    0.250    : Gendrisch2003
 6 f    6 e    1906337.903    0.250    : Gendrisch2003
 8 f    8 e    1919410.760    0.200    : Gendrisch2003
...
NQN
```

Remarks

- The manifolds can be defined either in the state definition (e.g. `LowerState X.030P`, as in the example above) or in line (e.g., `LowerManifold X000 / LowerState Sigma` using two lines).
- We report measurements from the literature in their given units, i.e., MHz or cm^{-1} . The `unit` command can be used to switch within the `obs` file.

4.3 Eigenvalues

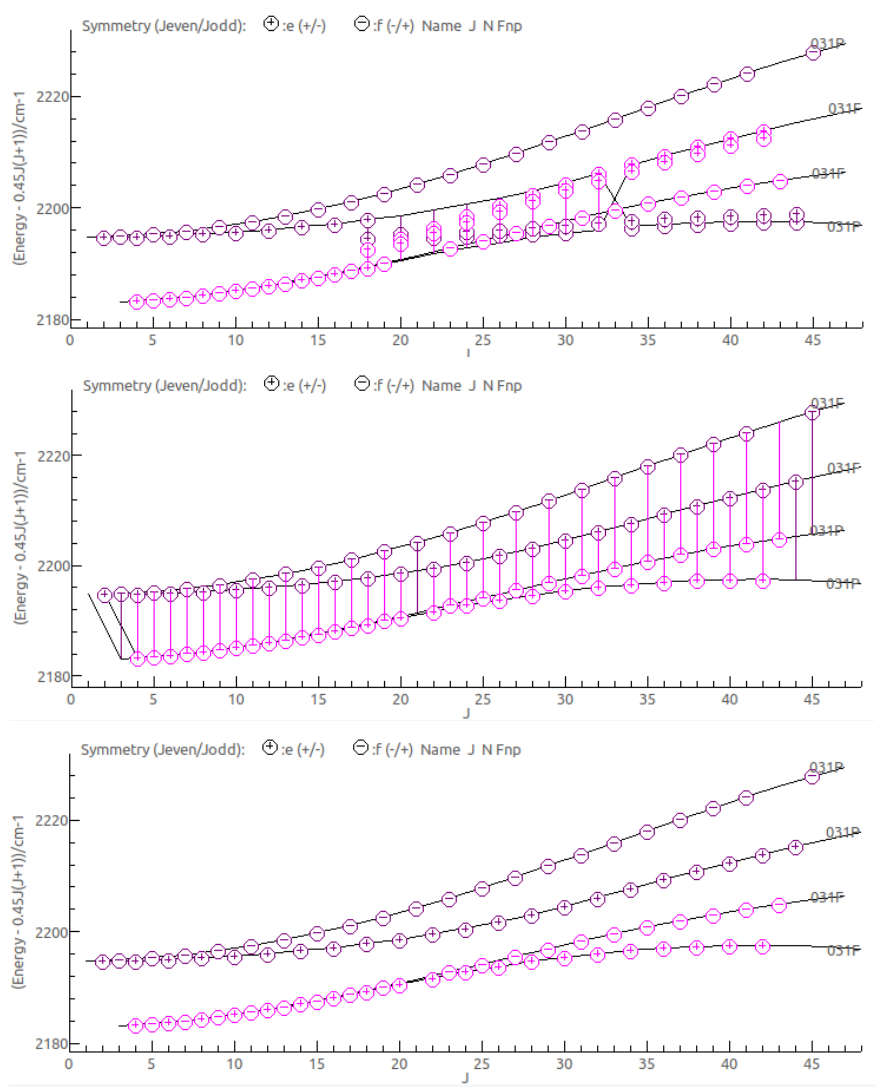
The EigenSearch option is a key parameter needed to properly fit C_3 . In each manifold, the EigenSearch option needs to be omitted (`EigenSearch = False`) so that the vibrational levels eigenvalues are not be renumbered for each J values. In case of crossing, it avoids discrepancies

between vibrational level name and eigenvalues (which are dealt with by PGOPHER, thus it remains transparent for the user).

In consequence, levels that are crossing each other need to appear in increasing energy order in the list. For example, for (030) in the electronic ground state, the Φ state has to be defined before the Π state.

Remark: The definition of “increasing” energy is not straightforward from the band center value, since it depends on the Hamiltonian definition (`RSquaredH = True` or `False`).

A straightforward way to verify that the PGOPHER file is set properly is to check the level plots ([View -> Levels](#)). The figure below presents the different that can arise from a bad definition of the eigenvalue associated to each state.



Importance of the eigenvalue search and level orders illustrated for the (031) levels of C_3 . The black lines represent the calculated levels, the colored circles are the level position resulting from the assignment (with spectroscopic constants at their final value). *Top trace:* `EigenSearch = True`. There is a crossing of levels between $J = 33$ and 35 . *Middle trace:* `EigenSearch = False` and Π defined before $\Phi \rightarrow$ the levels are swapped. *Bottom trace:* `EigenSearch = False` and Φ defined before $\Pi \rightarrow$ the levels are now properly defined.

References

- W. J. Balfour, J. Cao, C. V. V. Prasad, and C. X. W. Qian. Laser-induced fluorescence spectroscopy of the $\tilde{\Lambda}^1\Pi_u - \tilde{X}^1\Sigma_g^+$ transition in jet-cooled C_3 . *J. Chem. Phys.*, 101(12):10343–10349, 1994. doi: 10.1063/1.467914.
- A. A. Breier, T. Büchling, R. Schnierer, V. Lutter, G. W. Fuchs, K. M. T. Yamada, B. Mookerjea, J. Stutzki, and T. F. Giesen. Lowest bending mode of ^{13}C -substituted C_3 and an experimentally derived structure. *J. Chem. Phys.*, 145(23):234302, 2016. doi: 10.1063/1.4971854.
- A. J. de Nijs, E. J. Salumbides, K. S. E. Eikema, W. Ubachs, and H. L. Bethlem. UV-frequency metrology on CO ($a^3\Pi$): Isotope effects and sensitivity to a variation of the proton-to-electron mass ratio. *Phys. Rev. A*, 84:052509, 2011. doi: 10.1103/PhysRevA.84.052509.
- L. Gausset, G. Herzberg, A. Lagerqvist, and B. Rosen. Analysis of the 4050-ågroup of the C_3 molecule. *Astrophys. J.*, 142:45, 1965. doi: 10.1086/148262.
- R. Gendriesch, K. Pehl, T. Giesen, G. Winnewisser, and F. Lewen I. Terahertz Spectroscopy of Linear Triatomic CCC: High Precision Laboratory Measurement and Analysis of the Ro-Vibrational Bending Transitions. *Z. Naturforsch. A*, 58(2-3), 2003. doi: 10.1515/zna-2003-2-310.
- M. A. Haddad, D. Zhao, H. Linnartz, and W. Ubachs. Rotationally resolved spectra of the 4051 Å comet band of C_3 for all six ^{12}C and ^{13}C isotopologues. *J. Mol. Spectrosc.*, 297:41–50, 2014. doi: 10.1016/j.jms.2014.01.010.
- M. Izuha and K. Yamanouchi. New vibronic bands of the laser-vaporized C_3 cluster. Determination of the ν_3 fundamental in the $\tilde{\Lambda}^1\Pi_u$ state. *Chem. Phys. Lett.*, 242(4):435–442, 1995. doi: 10.1016/0009-2614(95)00758-V.
- M. Izuha and K. Yamanouchi. New $\tilde{\Lambda} - \tilde{X}$ Vibronic Bands of Laser-Vaporized C_3 . *J. Chem. Phys.*, 109(5):1810–1818, 1998. doi: 10.1063/1.476756.
- K. Kawaguchi, K. Matsumura, H. Kanamori, and E. Hirota. Diode laser spectroscopy of C_3 : The $\nu_2 + \nu_3 - \nu_2$, $2\nu_2 + \nu_3 - \nu_2$, and $2\nu_2 + \nu_3$ bands. *J. Chem. Phys.*, 91(4):1953–1957, 1989. doi: 10.1063/1.457054.
- J. Krieg, V. Lutter, C. P. Endres, I. H. Keppeler, P. Jensen, M. E. Harding, J. Vázquez, S. Schlemmer, T. F. Giesen, and S. Thorwirth. High-Resolution Spectroscopy of C_3 around 3 μm . *J. Phys. Chem. A*, 117(16):3332–3339, 2013. doi: 10.1021/jp3119204.
- K. Matsumura, H. Kanamori, K. Kawaguchi, and E. Hirota. Infrared diode laser kinetic spectroscopy of the ν_3 band of C_3 . *J. Chem. Phys.*, 89(6):3491–3494, 1988. doi: 10.1063/1.454919.
- B. McCall, R. Casaes, M. Ádámkovics, and R. Saykally. A Re-Examination of the 4051 Å Band of C_3 Using Cavity Ringdown Spectroscopy of a Supersonic Plasma. *Chem. Phys. Lett.*, 374(5-6): 583–586, 2003. doi: 10.1016/S0009-2614(03)00769-3.
- A. J. Merer. Absorption spectra of C_3 and $C_3\text{H}_2$ from the flash photolysis of diazopropane. *Can. J. Phys.*, 45(12):4103–4111, 1967. doi: 10.1139/p67-342.
- M. R. Schmidt, J. Krełowski, G. A. Galazutdinov, D. Zhao, M. A. Haddad, W. Ubachs, and H. Linnartz. Detection of vibronic bands of C_3 in a translucent cloud towards HD 169454. *Mon. Not. R. Astron. Soc.*, 441(2):1134–1146, 2014. doi: 10.1093/mnras/stu641.

- C. A. Schmuttenmaer, R. C. Cohen, N. Pugliano, J. R. Heath, A. L. Cooksy, K. L. Busarow, and R. J. Saykally. Tunable far-IR laser spectroscopy of jet-cooled carbon clusters: the ν_2 bending vibration of C₃. *Science*, 249(4971):897–900, 1990. doi: 10.1126/science.11538082.
- B. Schröder, K. D. Doney, P. Sebald, D. Zhao, and H. Linnartz. Stretching our understanding of c₃: Experimental and theoretical spectroscopy of highly excited $n\nu_1 + m\nu_3$ states ($n \leq 7$ and $m \leq 3$). *J. Chem. Phys.*, 149(1):014302, 2018. doi: 10.1063/1.5034092.
- A. Tanabashi, T. Hirao, T. Amano, and P. F. Bernath. Fourier Transform Emission Spectra of the (000)–(000) Band of the 4051.6 Band of C₃. *Astrophys. J.*, 624(2):1116–1120, 2005. doi: 10.1086/429316.
- D. W. Tokaryk and D. E. Chomiak. Laser spectroscopy of C₃: Stimulated emission and absorption spectra of the $\tilde{\text{A}}^1\Pi_u - \tilde{\text{X}}^1\Sigma_g^+$ transition. *J. Chem. Phys.*, 106(18):7600–7608, 1997. doi: 10.1063/1.473762.
- G. Zhang, K.-S. Chen, A. J. Merer, Y.-C. Hsu, W.-J. Chen, S. Shaji, and Y.-A. Liao. The 4051 Å band of C₃ (A¹ Π_u - X¹ Σ_g^+ , 000-000): Perturbed low-J lines and lifetime measurements. *J. Chem. Phys.*, 122(24):244308, 2005. doi: 10.1063/1.1928827.